

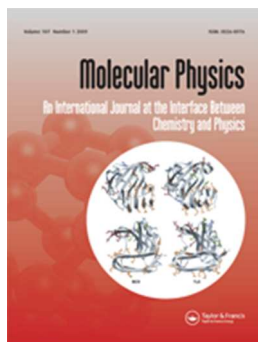


# MIT Open Access Articles

*The [ $\sim$  over  $A$ ]<sup>1</sup> $A$ <sub>u</sub> state of acetylene: ungerade vibrational levels in the region 45,800–46,550 cm<sup>-1</sup>*

The MIT Faculty has made this article openly available. **Please share** how this access benefits you. Your story matters.

<b>Citation</b>	Baraban, Joshua H., P. Bryan Changala, Anthony J. Merer, Adam H. Steeves, Hans A. Bechtel, and Robert W. Field. "The [ $\sim$ over $A$ ] <sup>1</sup> $A$ <sub>u</sub> State of Acetylene: Ungerade Vibrational Levels in the Region 45,800–46,550 cm <sup>-1</sup> ." Molecular Physics 110, no. 21–22 (November 2012): 2707–2723.
<b>As Published</b>	<a href="http://dx.doi.org/10.1080/00268976.2012.706329">http://dx.doi.org/10.1080/00268976.2012.706329</a>
<b>Publisher</b>	Taylor & Francis
<b>Version</b>	Author's final manuscript
<b>Citable link</b>	<a href="http://hdl.handle.net/1721.1/95912">http://hdl.handle.net/1721.1/95912</a>
<b>Terms of Use</b>	Creative Commons Attribution-Noncommercial-Share Alike
<b>Detailed Terms</b>	<a href="http://creativecommons.org/licenses/by-nc-sa/4.0/">http://creativecommons.org/licenses/by-nc-sa/4.0/</a>



**The  $\tilde{A}^1A_u$  state of acetylene: ungerade vibrational levels  
in the region 45800 – 46550  $\text{cm}^{-1}$**

Journal:	<i>Molecular Physics</i>
Manuscript ID:	TMPH-2012-0221.R1
Manuscript Type:	Special Issue - FASE
Date Submitted by the Author:	14-Jun-2012
Complete List of Authors:	Baraban, Joshua; MIT, Chemistry; Massachusetts Institute of Technology, Chemistry Changala, Peter; Massachusetts Institute of Technology, Chemistry Merer, Anthony; Institute of Atomic and Molecular Sciences, Academia Sinica, ; University of British Columbia, Chemistry Steeves, Adam; Massachusetts Institute of Technology, Chemistry Bechtel, Hans; Massachusetts Institute of Technology, Chemistry Field, Robert; MIT, Chemistry
Keywords:	acetylene, cis-trans isomerization, double resonance, spectroscopy, perturbations

SCHOLARONE™  
Manuscripts

1  
2  
3  
4  
5  
6  
7  
8  
9  
10  
11  
12  
13  
14  
15  
16  
17  
18  
19  
20  
21  
22  
23  
24  
25  
26  
27  
28  
29  
30  
31  
32  
33  
34  
35  
36  
37  
38  
39  
40  
41  
42  
43  
44  
45  
46  
47  
48  
49  
50  
51  
52  
53  
54  
55  
56  
57  
58  
59  
60

Dear Editor and Reviewer,

We would like to thank the referee for their helpful comments, and we have edited the manuscript and figures accordingly.

Sincerely,

Josh Baraban

Only

**The  $\tilde{A}^1A_u$  state of acetylene: ungerade vibrational levels  
in the region 45800 – 46550  $\text{cm}^{-1}$**

Joshua H. Baraban<sup>a</sup>, P. Bryan Changala<sup>a</sup>, Anthony J. Merer<sup>b,c</sup>, Adam H. Steeves<sup>a†</sup>,  
Hans A. Bechtel<sup>a\*</sup> and Robert W. Field<sup>a\*</sup>

\*Corresponding author. Email: [rwfield@mit.edu](mailto:rwfield@mit.edu)

<sup>a</sup>Department of Chemistry, Massachusetts Institute of Technology, Cambridge, MA 02139,  
U.S.A.; <sup>b</sup>Institute of Atomic and Molecular Sciences, Academia Sinica, Taipei 10617, Taiwan;

<sup>c</sup>Department of Chemistry, University of British Columbia, Vancouver, BC V6T 1Z1, Canada.

<sup>†</sup>Present address: Department of Pharmaceutical Chemistry, University of California at San  
Francisco, San Francisco, CA 94143, U.S.A.

<sup>‡</sup>Present address: Advanced Light Source Division, Lawrence Berkeley National Laboratory,  
Berkeley, CA 94720, U.S.A.

1  
2  
3  
4  
5  
6  
7  
8  
9  
10  
11  
12  
13  
14  
15  
16  
17  
18  
19  
20  
21  
22  
23  
24  
25  
26  
27  
28  
29  
30  
31  
32  
33  
34  
35  
36  
37  
38  
39  
40  
41  
42  
43  
44  
45  
46  
47  
48  
49  
50  
51  
52  
53  
54  
55  
56  
57  
58  
59  
60

**Abstract**

The *ungerade* vibrational levels of the  $\tilde{A}^1A_u$  ( $S_1$ -trans) state of  $C_2H_2$  lying in the region 45800–46550  $cm^{-1}$  have been assigned from IR-UV double resonance spectra. The aim has been to classify the complete manifold of  $S_1$ -trans levels in this region, so as to facilitate the assignment of the bands of  $S_1$ -cis  $C_2H_2$ . The rotational structure is complicated because of the overlapping of vibrational polyads with different Coriolis and Darling-Dennison parameters, but assignments have been possible with the help of predictions based on the properties of polyads at lower energy. An important result is that the analysis of the  $(1^1_4^1, 1^1_6^1)$  polyad determines the anharmonicity constants  $x_{14}$  and  $x_{16}$ , which will be needed to proceed to higher energies. Some regions of impressive complexity occur. Among these is the band given by the  $3^3_6^1$ ,  $K=1$  state at 45945  $cm^{-1}$ , where a three-level interaction within the  $S_1$  state is confused by triplet perturbations. Several probable  $S_1$ -cis states have been observed, including cis-6<sup>2</sup>,  $K=1$ ; this vibrational level appears to show a K-staggering, of the type that arises when quantum mechanical tunnelling through the barrier to cis-trans isomerization is possible. The total number of identified cis vibrational states is now 6 out of an expected 10 up to the energies discussed in this paper.

## 1. Introduction

It has been known for nearly 60 years [1-3] that the first absorption transition in the electronic spectrum of acetylene,  $\tilde{A}^1A_u - \tilde{X}^1\Sigma_g^+$ , goes from the ground state (where the molecule is linear) to an excited state where the molecule is trans-bent (point group  $C_{2h}$ ). Some years after the first analyses, *ab initio* calculations [4-9] showed that the excited electronic state,  $\tilde{A}$ , also supports a potential minimum corresponding to a cis-bent structure. Because the  $\tilde{A}$  state of the cis-bent structure transforms as  $^1A_2$  in the  $C_{2v}$  point group, it was thought that transitions from the ground state to it would never be observable, since  $^1A_2 - ^1\Sigma_g^+$  electronic transitions are forbidden by the electric dipole selection rules. Nevertheless, a recent detailed study of the vibrational structure of the  $\tilde{A}^1A_u - \tilde{X}^1\Sigma_g^+$  system [10] has identified some weak bands going to levels which cannot be fitted into the manifold of the  $\tilde{A}^1A_u$  ( $S_1$ -trans) state. The  $^{13}\text{C}$  isotope shifts, upper state lifetimes and rotational structures of these bands confirm that they belong to the  $\tilde{A}^1A_2$  ( $S_1$ -cis) state. [11]

The discovery of the  $S_1$ -cis state of acetylene opens up the very interesting possibility of studying the spectroscopic signature of cis-trans isomerization at high resolution. In the  $S_1$  state of  $\text{C}_2\text{H}_2$  the trans conformer is the more stable, with the separation of the cis and trans zero-point levels being about  $2700\text{ cm}^{-1}$ ; the barrier to isomerization is calculated to lie about  $2300\text{ cm}^{-1}$  above the cis zero-point level. [12] The molecule is predicted [4] to be half-linear at the saddle point, with one of the CCH angles near  $120^\circ$ , and the other near  $180^\circ$ . Since the barrier to isomerization is not unduly high, the vibrational structure is not hopelessly dense at the saddle point, so that many vibrational assignments can be made with some certainty. However, the arguments that lead to these assignments are not trivial.

There are a number of complicating factors. The “isomerization pathway”, which the molecule follows in going from its trans equilibrium structure to the half-linear structure at the transition state, is a combination of the vibrational normal coordinates  $Q_3$  (trans bend) and  $Q_6$  (cis bend). Since the pathway leads to a saddle point on the potential surface, the result is huge anharmonicity in the combination levels  $3^m6^n$ , represented by large values of  $x_{36}$  and the higher anharmonicity constants. [13,1914] The most severe problem in identifying the levels is that  $\nu_6$  is inextricably bound up with  $\nu_4$  (torsion) as a result of the vibrational angular momentum, which causes levels of these vibrations to interact by two different mechanisms. The two fundamentals  $\nu_4$  and  $\nu_6$  lie at  $764.9$  and  $768.3\text{ cm}^{-1}$ , respectively, and interact strongly through both a- and b-axis Coriolis coupling ( $\zeta_{46}^a = 0.70$ ,  $\zeta_{46}^b = 0.71$ ). [154] In addition to the Coriolis coupling, the overtones also suffer from unusually strong Darling-Dennison resonance ( $K_{4466} = -51.7\text{ cm}^{-1}$ ). [165] The result is that the vibrational levels involving  $\nu_4$  and  $\nu_6$  form polyads of interacting levels, where the levels have the same value of  $\nu_4 + \nu_6$ . These polyads have highly irregular vibrational and rotational structures, which can only be reproduced with detailed numerical simulations. Fortunately,  $\nu_3'$  is the principal Franck-Condon active vibration in the electronic transition, [1-3,176,187] which means that many of the combination levels  $3^m6^n$  carry sizeable

intensities. Also, it turns out that some systematic patterns can be recognized in the various polyads. For example, the structures of those polyads which differ only in their values of  $\nu_4 + \nu_6$  can be represented approximately by a single set of effective vibrational and anharmonicity constants. [165] This has been the key to making assignments at progressively higher energies.

The present paper reports analyses of the *ungerade* vibrational levels in the region 45800 – 46500  $\text{cm}^{-1}$ , as observed in IR-UV double resonance. The objective of the work has been to establish secure assignments of *all* the trans levels in this region so that any levels left over can confidently be assigned to the cis conformer. The region studied is one of considerable complexity, containing 22 more or less strongly interacting vibrational levels from the trans manifold and 4 levels from the cis manifold. Two of these four are newly identified.

## 2. Experimental details

The rotational selection rule  $K' - l'' = \pm 1$  for the electronic transition necessitated two sets of double resonance experiments in order to sample all of the levels with  $K'=0-2$ . In one, the  $\nu_3$  IR fundamental ( $l'' = 0$ ) gave access to the  $K' = 1$  upper levels; in the other, the combination levels  $\nu_3 + \nu_4$  and  $\nu_1 + \nu_5$  ( $l'' = 1$ ) gave access to the  $K' = 0$  and 2 levels.

The  $\nu_3 + \nu_4$  and  $\nu_1 + \nu_5$ -pumped spectra analyzed in this paper are the same as those reported in Refs. [10] and [165]. As Ref. [10] contains the complete experimental details, only a summary of those IR-UV double resonance experiments will be given here. Difference frequency generation in a  $\text{LiNbO}_3$  crystal pumped by an injection-seeded Nd:YAG laser (Spectra-Physics PRO-270) at 1064 nm and a tunable dye laser (Lambda Physik FL2002) at 740-790 nm produced the IR radiation, which was amplified in a second  $\text{LiNbO}_3$  crystal to about 3 mJ/pulse. The UV radiation was generated by a second dye laser (Lambda Physik FL3002E) pumped by the third harmonic of an Nd:YAG laser (Spectra-Physics DCR-3). Most of the dye laser output was frequency-doubled in a  $\beta$ -barium borate crystal, while a small portion of the fundamental was passed through a heated  $^{130}\text{Te}_2$  vapor cell for frequency calibration ( $\sigma = 0.02 \text{ cm}^{-1}$ ). The IR and UV radiation were sent into a molecular beam chamber where they interacted with an unskimmed jet of neat acetylene expanded through a pulsed valve (General Valve, Series 9) with a backing pressure of 2 atm. The laser-induced fluorescence was observed at an angle mutually perpendicular to the laser path and molecular beam and recorded by a Hamamatsu R331 photomultiplier tube.

The newly recorded  $\nu_3$ -pumped spectra were obtained in a separate apparatus from that used in the recording of the  $\nu_3 + \nu_4$  and  $\nu_1 + \nu_5$ -pumped spectra. A single injection-seeded Nd:YAG laser (Spectra-Physics PRO-270) pumped the two tunable dye lasers for both IR and UV generation. The Nd:YAG second harmonic at 532 nm pumped the first dye-laser (Lambda Physik FL2002) operating at 790 nm (LDS 798 dye). As above, this output, along with the

Nd:YAG fundamental at 1064 nm, pumped a LiNbO<sub>3</sub> crystal producing IR radiation via difference frequency generation. Approximately 1.5 mJ/pulse was achieved through the difference frequency generation alone, and this IR beam was not amplified with a second LiNbO<sub>3</sub> crystal. To ensure the resonance of the IR frequency with transitions in the  $\nu_3$  fundamental band [20], a photoacoustic cell with 15 torr of neat acetylene gas at room temperature was monitored before each IR-UV double resonance experiment. The grating-limited IR spectral width was 0.10 cm<sup>-1</sup>.

The Nd:YAG third harmonic at 355 nm pumped the second dye-laser (Lambda Physik FL3002E) to produce laser radiation over the range 460-470 nm (Coumarin 460 dye). This output was doubled with a  $\beta$ -barium borate crystal and, as above, a small portion of the fundamental was used for <sup>130</sup>Te<sub>2</sub> frequency calibration. An intracavity etalon reduced the spectral width to 0.04 cm<sup>-1</sup>, and after frequency-doubling, the UV power was approximately 100-200  $\mu$ J/pulse. The IR and UV beams were recombined with a dichroic mirror before entering the molecular beam chamber. As a single Nd:YAG laser generated both pulses, their relative arrival times at the chamber could be controlled only through the addition of a delay line in the UV beam path. The length of the delay line was such that the UV pulse arrived 15 ns after the IR pulse.

The molecular beam chamber contained an unskimmed supersonic jet of neat acetylene expanded through one of two pulsed valves (Jordan PSV C-21,  $d = 0.5$  mm or General Valve, Series 9,  $d = 1.0$  mm). The latter achieved superior vibrational cooling, necessary when single-photon hot-bands obscured overlapping IR-UV double resonance features in the spectrum. In both cases, the jet was backed by a pressure of 1 atm and interacted with the IR-UV radiation about 2 cm from the nozzle. The diffusion pumped chamber achieved an ultimate pressure of  $7 \times 10^{-7}$  torr, while under gas load it rose to  $0.5\text{--}2 \times 10^{-5}$  torr.

A Hamamatsu R375 photomultiplier tube collected the laser-induced fluorescence using  $f/1.2$  collection optics and a UG-11 filter to block laser scatter. Additionally, optical baffles consisting of a set of 3.5 mm aperture irises placed 9" from the interaction region and a second set of 5.5 mm aperture irises placed 4" from the interaction region were installed in the entrance and exit window arms of the chamber, which significantly reduced laser scatter. The photomultiplier tube signal was split and one line was input to a 30 dB voltage amplifier (Femto DHPVA-200). This was necessary as the fluorescence intensity of levels in the studied energy region range varied over several orders of magnitude. The time-dependent fluorescence signal was recorded for 2  $\mu$ s after the UV pulse arrival time. For each frequency resolution element, the fluorescence signal was averaged for 20 laser shots. The integration gate of the time signal could be chosen depending on the fluorescent lifetime of the final state. Typically, the fluorescence signal over the first 0.4  $\mu$ s after the UV laser pulse was integrated. However, for short-lived states this integration gate had to be moved earlier in time and included the UV laser



pulse scatter. In this case, the laser scatter and power fluctuations were small enough not to contribute significantly to the integrated signal noise.

Since the  $\nu_3$  fundamental is a parallel band, IR pumping of individual R and P lines gives  $J''$ -selectivity. In contrast, the narrow Q branches of the perpendicular transitions to the  $\nu_3+\nu_4$  and  $\nu_1+\nu_5$  combination levels allow pumping of the  $J = 1f-5f$  levels simultaneously. This speeds up the data acquisition process, but loses the  $J$ -selectivity. As a result it was sometimes difficult to be certain of the rotational assignments of weaker lines in dense regions of the Q-pumped IR-UV double resonance spectra.

### 3. Appearance of the spectra

As observed by IR-UV double resonance, the region  $45800 - 46500 \text{ cm}^{-1}$  consists of congested overlapping structure centred on the very intense  $3^36^1$  band at  $45938 \text{ cm}^{-1}$ , with sparser structure to higher frequency. A survey spectrum is given in Fig. 1 of [10]. The congested region contains 15 vibrational levels from the trans manifold, together with two cis levels. One of the cis levels is  $\text{cis-}3^16^1$ , which was described in [11]. The trans levels are  $3^15^1$  and the polyads  $3^3B^1$ ,  $1^1B^1$ ,  $2^1B^3$  and  $B^5$ . (The notation  $B^n$  means  $n$  quanta of the bending vibrations, where  $n = \nu_4 + \nu_6$ ; a polyad  $B^n$  consists of  $n+1$  vibrational levels.) Three of the  $K$  states from the  $B^5$  polyad were described in [11,165], and analyses of the  $3^15^1$  state [198] and the  $3^3B^1$  polyad [13] have been reported by other workers, but no previous attempts have been made to assign the remainder of the congested region. The sparse region contains the  $2^15^1$  state and the polyads  $3^2B^3$  and  $2^13^2B^1$ , together with two new cis levels. There are surprising numbers of accidental near-degeneracies among the upper states, which result in some wickedly complicated spectra.

Because the rotational selection rule  $K' - l'' = \pm 1$  requires separate experiments for the even- $K$  and odd- $K$  upper states, no single spectrum can illustrate the complete level pattern. To be sure, many of the  $K$  states show up in both spectra when  $b$ -axis Coriolis interaction mixes close-lying levels differing in  $K$  by one unit, but the intensities of the bands are not representative in those cases. Figure 1 gives a stick diagram of the  $K' = 0 - 2$  structure in the congested region around  $46000 \text{ cm}^{-1}$ , as observed in the two spectra, with approximate intensities indicated by the heights of the sticks. A common feature of all the polyads, particularly those with  $\nu_4 + \nu_6 > 1$ , is that the vibrational and rotational structure is much denser at the low frequency extreme than at higher frequencies. This level density effect at low frequency is a consequence of the  $a$ -axis Coriolis coupling, which depresses the lower members of the polyad with  $K > 0$ . Where Darling-Dennison resonance is also present, this density effect is enhanced. The  $2^1B^3$  polyad, shown in Fig. 1, is a good example of this. Figure 1 also shows how the congestion of the structure in the  $45800 - 45950 \text{ cm}^{-1}$  region results from overlapping of the low frequency extremes of three polyads.

The lower part of Figure 1 shows the assignments of the levels to the various polyads. Except in one instance where two  $K=2$  levels are almost degenerate, the assignments are unambiguous, because it has been possible to predict the positions of the levels to within a few  $\text{cm}^{-1}$ , using data from previous analyses of polyads at lower energy. These predictions are described below.

#### 4. Results

As yet, no attempt has been made to fit all of the interacting levels of Fig. 1 simultaneously by least squares. **Table 1** lists rotational constants obtained from band-by-band fitting of the 60 observed  $K'$  upper states. It has not been possible to obtain meaningful constants for every  $K$  state either because the bands are too weak, or because of perturbations. In the latter cases, a separate discussion of the interactions is given.

##### 4.1 Predictions of the vibrational and rotational structures of the polyads

As indicated above, the assignments of the  $K$  states could be made following predictions of the vibrational and rotational structures based on constants derived from polyads at lower energy. It was found in [165] that the pure bending polyads could all be represented with fair accuracy by a single set of vibrational and anharmonicity parameters. This allowed predictions and assignments to be made for the three  $K$  states of the  $B^5$  polyad observed in that work, based on the parameters from detailed least squares fitting of the  $B^1$ ,  $B^2$  and  $B^3$  polyads. In the present work, where the rest of the  $B^5$  polyad has been assigned, the predictions of [165] were used again, and were found to be accurate to within  $7 \text{ cm}^{-1}$  for all the observed  $K = 0 - 2$  states. Greater accuracy should not be expected since it is known that Fermi resonances of the type  $\Delta v_2 = \pm 1$ ,  $\Delta v_B = \mp 2$  are present. Nevertheless the shifts caused by these resonances are quite small, except in one instance. The lowest  $K=0$ ,  $B_u$  level of the  $B^5$  polyad is predicted to lie  $20 \text{ cm}^{-1}$  below the corresponding  $K=0$ ,  $A_u$  level, but is found experimentally to lie  $29 \text{ cm}^{-1}$  below it. It happens that the top  $K=0$ ,  $B_u$  and  $A_u$  levels of the  $2^1B^3$  polyad lie in the gap between the two  $B^5$  levels. Fermi resonance then pushes the  $B^5$ ,  $B_u$  level further down and the  $B^5$ ,  $A_u$  level further up. At the same time, the  $B_u$  and  $A_u$  levels of the  $2^1B^3$  polyad, which in the absence of the resonance are predicted to lie in the energy order  $B_u$  below  $A_u$ , end up with the  $A_u$  level  $3 \text{ cm}^{-1}$  below the  $B_u$  level. The resulting level pattern can be understood from Fig. 1.

It turns out that the combination stretch-bend polyads behave similarly to the pure bending polyads. For example, from the least squares results for the  $3^2$ ,  $3^2B^1$  and  $3^2B^2$  level positions [10,13,176], it is possible to derive a set of effective vibrational and anharmonicity parameters that gives the basis for a prediction of the  $3^2B^3$  polyad:

$$\omega_4 = 739.93, \quad x_{44} = 0.43, \quad \omega_6 = 712.765, \\ x_{66} = -11.715, \quad x_{46} = 19.38, \quad K_{4466} = -66.50 \quad (\text{all in } \text{cm}^{-1})$$

$$\zeta_{46}^a = 0.77, \zeta_{46}^b = 0.638. \quad (1)$$

Taking the rotational constants from the lower polyads, this set predicts the K levels of the  $3^2B^3$  polyad to within  $10 \text{ cm}^{-1}$ . The resulting assignments are clear-cut, except for a pair of bands near  $46415 \text{ cm}^{-1}$ , where there is a near-degeneracy (to within  $2 \text{ cm}^{-1}$ ) with a level from the  $2^13^2B^1$  polyad. It is interesting that the predictions for the  $3^2B^3$  polyad are not as accurate as those for the  $B^5$  polyad; the levels in question lie closer to the barrier to cis-trans isomerization, and it may be that the effects of tunnelling through it are already evident.

The predictions used in this work were full calculations of the rotational and vibrational structures of the polyads, based on a matrix treatment of the rotation, Coriolis coupling, and Darling-Dennison resonance. The matrix elements have been described in detail in [165], and are not repeated here.

At the start of this work it was not known whether the lowest K states in the  $45800 \text{ cm}^{-1}$  region belong to the  $1^1B^1$  polyad or to the  $2^1B^3$  polyad. The answer was supplied by *ab initio* calculations [149] of the anharmonicity parameters  $x_{14}$  and  $x_{16}$ , and confirmed later by arguments of the type just described. For these two parameters, the *ab initio* results gave  $-16.1$  and  $-9.8 \text{ cm}^{-1}$ , respectively, while the experimental values (taking the  $1^1B^1$  polyad as the higher of the two, as in Fig. 1) are  $-16.7$  and  $-11.6 \text{ cm}^{-1}$ ; the alternative assignment, with the  $1^1B^1$  polyad as the lower of the two, gives  $x_{14}$  and  $x_{16}$  as  $-31.9$  and  $-35.0 \text{ cm}^{-1}$ , respectively.

#### 4.2 $K'=0-2$ levels in the region $45800 - 45880 \text{ cm}^{-1}$

The lowest  $K'=0-2$  levels of the  $1^1B^1$  and  $2^1B^3$  polyads lie in the region  $45800-45880 \text{ cm}^{-1}$ . The b-axis Coriolis interactions are sufficiently strong that almost every  $K'$  state appears in the double resonance spectra from *both*  $v_3''$  ( $l=0$ ) and  $(v_3+v_4)''$  ( $l=1$ ), regardless of its  $K'$  value. For both polyads, the lowest level is a  $K'=1$  level, as is frequently the case in the bending polyads when  $v_3$  is not excited. The next levels in each polyad are a pair of  $K'=0$  levels, with  $A_u$  and  $B_u$  symmetries. These two  $K'=0$  levels are  $8.4 \text{ cm}^{-1}$  apart for  $1^1B^1$ , but only  $0.2 \text{ cm}^{-1}$  apart for  $2^1B^3$ . This difference arises because the  $2^1B^3$  polyad is subject to Darling-Dennison resonance, whereas the  $1^1B^1$  polyad is not. The  $A_u$  level lies below the  $B_u$  level in both polyads, as expected when  $v_3$  is not excited.

The energy level pattern of the ten lowest levels is illustrated in Fig. 2, where the reduced rotational levels are plotted against  $J(J+1)$ . A remarkably strong b-axis Coriolis interaction occurs between the second  $K=1$  and  $K=2$  levels of the  $2^1B^3$  polyad (illustrated at the top of the figure). The lower of the two resulting levels has an apparent B rotational constant of  $0.6 \text{ cm}^{-1}$ , compared to  $1.07 \text{ cm}^{-1}$  for an unperturbed level. This means that it falls rapidly in energy, relative to the levels nearby, and passes through the  $K=0$ ,  $B_u$  level of  $1^1B^1$ , causing a small perturbation. At  $J=6$  it runs into another interaction, with the lowest  $K=2$  level of the polyad.

The corresponding band has a very unusual appearance, with the R branch forming a head at  $J''=1$  in double resonance via  $\nu_3''$ . This band is illustrated in **Fig. 3**, where it is labelled 45838  $K=1$ . Fig. 3 also shows the band given by the  $K=2$  level which interacts with it. This is labelled 45842  $K=2$ ; its branches have unusual spacings at low  $J$ . A somewhat similar Coriolis interaction occurs in the  $B^3$  polyad, [165] though not in  $3^1B^3$ .

Two close-lying  $K'=1$  levels at 45860 and 45864  $\text{cm}^{-1}$  ( $1^1B^1$ ,  $K=1$  (II) and  $2^1B^3$ ,  $K=1$  (III)) give strong bands in the  $\nu_3$  double resonance spectra, but only very weak features in the  $\nu_3+\nu_4$  spectra. (The Roman numeral notation gives the ascending energy order for their  $K$  value within the polyad.) The predictions place the  $1^1B^1$ ,  $K=1$  (II) level just 1  $\text{cm}^{-1}$  below the  $2^1B^3$ ,  $K=1$  (III) level but, since the predictions are accurate only to about  $\pm 4 \text{ cm}^{-1}$  for any given level, it was not possible initially to be sure of the assignments. A similar situation occurs with the  $K=2$  levels at 45912 and 45915  $\text{cm}^{-1}$ , which can be assigned from the predictions as  $1^1B^1$ ,  $K=2$  (II) and  $B^5$ ,  $K=2$  (I), though without it being possible to decide which is which. However, all the  $K'$  states expected in this region have been found, so that we potentially have data for all six of the  $1^1B^1$ ,  $K=0-2$  states, and can subject these levels to a least squares fit. Interestingly, after examining the various possibilities, the conclusions drawn from the least squares fit are very clear: the lower of the two  $K=1$  levels is  $1^1B^1$ , as is the lower of the two  $K=2$  levels.

#### 4.3 $K'=0-2$ levels in the region 45890 - 45990 $\text{cm}^{-1}$

The region 45890 - 45990  $\text{cm}^{-1}$  contains the  $3^36^1$  level, which gives very intense bands, [13,21] together with the dense group of levels at the low frequency extreme of the  $B^5$  polyad. It seems that anharmonic resonances transfer intensity from the  $3^36^1$  level to *all* the other levels nearby, so that the resulting spectrum is strong but crowded. Fifteen states with  $K'=0-2$  are predicted in this region, and all are observed. There are no major perturbations except in the  $3^36^1$  vibrational level, where all the  $K'$  states show small splittings as a result of interaction with the "background" of triplet levels. The  $3^36^1$ ,  $K'=1$  state has a particularly large number of triplet perturbations, and is also involved in a three level interaction with states from the  $B^5$  polyad.

The spectrum given by the  $3^36^1$ ,  $K'=1$  state, as seen in double resonance via the  $J''=0-5$  levels of the  $\nu_3''$  fundamental, is illustrated in **Fig. 4**. In order not to confuse the patterns, some overlapping lines from the  $3^36^1$ ,  $K'=0$  state at 45937  $\text{cm}^{-1}$  and the  $B^5$ ,  $K'=1$  state at 45931  $\text{cm}^{-1}$  are shown with dots. In the absence of perturbations, the spectrum would consist of an R, a Q and a P line for each  $J''$  value but, as the figure shows, all the lines are split into several components, usually forming three main groups. A prominent interval of 1-2  $\text{cm}^{-1}$  appears in most of the groups of lines. Many of the lines are surrounded by a background of weak unresolved structure, which may extend for up to 1  $\text{cm}^{-1}$ . The background levels are presumably from the triplet manifold, which is expected to be extremely dense at this energy [22]. Most of the lines give extremely long lifetimes (1-3  $\mu\text{s}$  or more), and several exhibit strong zero-field

quantum beats. The R(0) line is especially interesting. It consists of two very strong lines, separated by  $0.31 \text{ cm}^{-1}$ , surrounded by about eight weaker features spread over more than  $2 \text{ cm}^{-1}$ . The two strong lines have almost exactly the same intensity, which implies that the zero-order  $3^3 6^1$ ,  $J'=1$  level is to high accuracy degenerate with a background  $J'=1$  level. Combination differences between the components of the R(0) and P(2) lines, which go to the same upper levels, show that the background of weaker features is real. The spacing of these levels gives an idea of how dense the triplet manifold actually is.

The observed upper state energy levels are shown, plotted against  $J(J+1)$  and with suitable reduction, in Fig. 5. The sizes of the symbols in Fig. 5 are rough representations of the intensities of the features in Fig. 4. Curves have been drawn through the centres of gravity of the strongest features. These curves show that there is a second zero-order vibrational level of the  $S_1$ -trans state in this energy range, and that it undergoes an avoided crossing with  $3^3 6^1$ ,  $K'=1$  between  $J' = 3$  and 4. This second set of rotational levels begins at  $J'=2$ , indicating that it belongs to a  $K=2$  state, but the avoided crossing pattern is somewhat unusual, because the slopes of the rotational energy curves are not the same before and after the crossing. As we shall see, the perturbing state is  $B^5$ ,  $K=2$  (II), which is itself perturbed. The triplet perturbations are clearly associated with the zero-order  $3^3 6^1$  state, because at the avoided crossing they transfer from the top set of levels to the next set down, following the state with  $3^3 6^1$  character.

A third set of energy levels is shown as a dotted line at the lower right hand side of Fig. 5. The upper states have comparatively short lifetimes, closer to the nominal  $S_1$  lifetime of 300 ns, and the lines at higher  $J$  values are sharper than those of the interacting  $3^3 6^1$ ,  $K=1$  and  $B^5$ ,  $K=2$  (II) states, indicating that they are less affected by the background of triplet levels. This implies that they belong to the  $S_1$  state. The  $K'$  value of the upper state is either 3 or 4, depending on whether or not there is a  $J=3$  level blended with  $B^5$ ,  $K=2$ ,  $J=3$ . We offer no assignment if the upper state has  $K=3$ , but for  $K=4$  there is a good match with the  $2^2 B^1$ ,  $K=4$  (II) state, which is calculated to lie near  $44952 \text{ cm}^{-1}$ , only  $8 \text{ cm}^{-1}$  above.

Detailed examination of the spectrum in Fig. 4 shows that Fig. 5 is not the whole story. In Fig. 4 the components of the lines with  $J'=2$  are marked with tie-lines. The low frequency components correspond to the  $J'=2$ ,  $K'=2$  levels shown at the bottom of Fig. 5. However the Q(2) and P(3) groups contain an additional line for which there is no counterpart in the R(1) pattern. These additional lines turn out to belong to a  $K'=3$  state, which is interacting with the  $K'=2$  state.

As Fig. 1 shows, the only polyad that could give perturbing states in this region is  $B^5$ . The pattern of its states can be predicted from the constants for the  $B^n$  polyads given in [165]. The observed and predicted level structure in this region, plotted against  $J(J+1)$ , is shown in Fig. 6. (An offset of  $3 \text{ cm}^{-1}$  has been added to the predictions since the extrapolation from the polyads with lower  $n = v_4 + v_6$  is not exact.) The levels from Fig. 5, but without the triplet structure, appear at the top of this figure. Figure 6 shows that the  $B^5$ ,  $K'=2$  (II) state interacts

strongly with the  $B^5$ ,  $K'=3$  (I) state, just below. At  $J'=3$  the separation of the  $K'=2$  and 3 states is calculated to be  $7.8 \text{ cm}^{-1}$ , which suggests that the additional lines in the Q(2) and P(3) patterns of Fig. 4 (which are  $7.1 \text{ cm}^{-1}$  apart) are R and Q lines going to the  $K'=3$  state. Combination differences confirm this assignment. Some higher-J Q lines going to the  $K'=3$  state are also marked in Fig. 4; the “observed”  $K'=3$  levels shown in Fig. 6 correspond to them.

Immediately below the  $K'=3$  state is the  $B^5$ ,  $K=1$  (II) state. The curvature of its plot in Fig. 6 shows that it is also involved in the interaction scheme. It gives rise to quite intense bands at  $45931 \text{ cm}^{-1}$  in both the  $\nu_3''$  and  $(\nu_3+\nu_4)''$  double resonance spectra, showing that the “goodness” of the quantum number  $K$  is severely compromised by Coriolis effects. Some of the lines shown as dashedotted in Fig. 4 are lines of its R branch.

The parabola-like energy level pattern given by the  $K'=2$  and 3 states in Fig. 6 is characteristic of a b-axis Coriolis ( $J$ -dependent) interaction between two states that are almost degenerate in zero-order. In this case the interaction is strong because the  $K'=2$  (II) and  $K'=3$  (I) states belong to nominally different vibrational components of the polyad, as indicated by the Roman numerals.

We note that the  $1\text{--}2 \text{ cm}^{-1}$  splitting of the  $J \geq 2$  levels of the  $3^36^1$ ,  $K'=1$  state reported in previous work [13,21] is not the result of triplet perturbations, but represents an avoided crossing with another vibrational level within the  $S_1$ -trans state. There are triplet perturbations in addition to the avoided crossing, but these are much smaller, and are centred on the  $3^36^1$ ,  $K=1$  state rather than its perturbing partner,  $B^5$ ,  $K=2$  (II). The interaction between the  $3^36^1$ ,  $K=1$  and  $B^5$ ,  $K=2$  (II) states is an extremely high-order resonance, representing a difference of at least seven quanta of vibration between the interacting states; consistent with this, the matrix element is only about  $0.5 \text{ cm}^{-1}$ .

Although there are no other avoided crossings among the states in this energy region, there are some interesting near degeneracies. For example, the  $2^1B^3$ ,  $K=2$  (III) and  $B^5$ ,  $K=1$  (I) states, near  $45896 \text{ cm}^{-1}$ , lie only  $0.4 \text{ cm}^{-1}$  apart at zero rotation. Clearly they interact quite strongly, apparently by a b-axis Coriolis mechanism, because the rotational levels are already  $2.8 \text{ cm}^{-1}$  apart at  $J=5$ . Because they belong to different polyads they should not interact at all, but the fact that they do is a result of Fermi resonance. This particular resonance occurs also between the  $2^13^1B^1$  and  $3^1B^3$  polyads, where the interaction parameters were determined by least squares [10] to be  $k_{244} = -7 \text{ cm}^{-1}$  and  $k_{266} = 8.7 \text{ cm}^{-1}$ . No attempt has been made to fit the two polyads simultaneously in the present instance, but it should be possible to refine the Fermi resonance parameters from the data for these states.

The same type of Fermi resonance occurs between the  $K'=0$  states belonging to  $2^1B^3$  and  $B^5$  near  $45900 \text{ cm}^{-1}$ ; this was described in Section 4.1. Surprisingly, the  $2^1B^3$ ,  $K=0$   $A_u$  and  $B_u$  states give very much weaker bands than the  $B^5$ ,  $K=0$   $A_u$  and  $B_u$  states, despite the resonance. By contrast, the nearby  $2^1B^3$ ,  $K=2$  (III) state gives reasonably strong bands, in spectra from both



$(\nu_3+\nu_4)''$  and  $\nu_3''$ , though it is possible that its intensity is enhanced by the b-axis interaction with  $B^5$ ,  $K=1$  (I) just described. Throughout the spectra the relative intensities of the various bands are not always easy to understand. An important contributing factor appears to be the interference between vibrational transition moments that occurs when the vibrational wave functions are far from harmonic as a result of the Coriolis and Darling-Dennison resonances. The Fermi resonances seem to be a less important factor, though their effects are unpredictable in the presence of the other resonances. Predissociation also begins to affect the intensities midway through this region.

The  $3^36^1$ ,  $K'=2$  state (at  $45972\text{ cm}^{-1}$ ) displays extensive triplet perturbations, but without the complication found in the  $K'=1$  state of an avoided crossing within the  $S_1$  state. In all cases where triplet perturbations are seen in our spectra it is found that at low  $J'$  values a nominal- $S_1$  line is split into a few well-separated components, with spacings of typically  $0.2\text{ cm}^{-1}$ . With increasing  $J'$  the number of components grows; they become closer together, and quickly coalesce into a single broad line. This represents the increasing density of the background triplet levels with increasing  $J'$ . At higher  $J$  values the lines become apparently sharper, as interactions with triplet levels within the line profile dominate, though weak outliers have been observed as much as  $0.4\text{ cm}^{-1}$  away. This is the pattern found in the  $3^36^1$ ,  $K=2$  state. The  $J'=2$  level has four recognizable components for both parities, but the splitting patterns are not the same. The  $J'=3$  lines have at least five components, though they are not well resolved, while the  $J'=6$  features look like single lines.

It has been possible to assign nearly all the observed lines in this region by combining data obtained via  $\nu_3''$  and  $(\nu_3+\nu_4)''$ . A few weaker lines remain unassigned, particularly in among the very intense bands from  $3^36^1$ , as seen via  $(\nu_3+\nu_4)''$ . Predictions of the expected structure show that some of these lines must be Coriolis-induced transitions to  $K'=3$  states, but the severe blending has made it impossible to obtain secure assignments.

#### 4.4 $K'=0-2$ levels in the region $46000 - 46250\text{ cm}^{-1}$

The region  $46000 - 46250\text{ cm}^{-1}$  contains the  $K'=0-2$  states from the  $3^34^1$  [13] and  $3^15^1$  [198] vibrational levels, together with eight states from the  $B^5$  polyad. Bands from two cis vibrational levels, cis- $6^2$  and cis- $3^16^1$  are also found; the cis- $6^2$   $K=0$  and the cis- $3^16^1$  bands have already been described in [11], but the cis- $6^2$ ,  $K=1$  band is new.

The  $3^34^1$  vibrational level gives the most intense bands in this region. In contrast to the  $3^36^1$  vibrational level, which suffers from exceptionally large numbers of perturbing triplet states, the  $3^34^1$  vibrational level is only mildly perturbed by triplets. Surface electron ejection by laser-excited metastables (SEELM) spectra have recently documented [22] the perturbations in both of the  $K'=0$  states, but perturbations have not been found previously for the  $3^34^1$ ,  $K'=1$  and 2

states. [13,21] Our spectra show that all three states with  $K'=0-2$  are perturbed at low  $J$ . The  $K'=0$  state gives only a Q branch in double resonance via  $(\nu_3+\nu_4)''$ , but extra lines are seen in our spectra accompanying the Q(1) – Q(3) lines, consistent with the SEELEM results. The  $K'=1$  state gives a weak band fragment in double resonance via  $(\nu_3+\nu_4)''$ , but an intense band via  $\nu_3''$ . Although the two parity components of the  $J'=1$  level appear at first sight to give single sharp lines, least squares fitting shows that they are both out of place. Weak extra lines can then be identified, lying within  $0.4\text{ cm}^{-1}$  of the main lines. The extra  $e$  symmetry levels lie above their main level, but the extra  $f$  level lies below its main level. The  $3^3_4^1$ ,  $K'=2$  state ( $46105\text{ cm}^{-1}$ ) also shows extra lines and other small irregularities which become obvious in the least squares fitting. The analysis is quite complicated because, for zero rotation, this state lies less than  $0.5\text{ cm}^{-1}$  above the  $3^1_5^1$ ,  $K=1$  state, which is itself perturbed by triplet levels. In the  $(\nu_3+\nu_4)''$  spectra the complications are compounded by an overlapping one-photon artifact, but the details are clearer in the  $\nu_3''$  spectra.

The triplet perturbations found in the  $3^1_5^1$  vibrational level affect just the  $K=1$ ,  $J=5e$  level, which is split into at least four components spread over more than  $0.7\text{ cm}^{-1}$ . Every triplet perturbation found so far in the  $S_1$  state appears in a level where  $\nu_3$  is involved, but this is the first example of a triplet perturbation in a level involving  $\nu_5$  (the antisymmetric CH stretching vibration).

It is interesting that the IR-UV double resonance spectra of the  $3^1_5^1$  level recorded by Tobiasson *et al.* [198] via the  $3\nu_3''$  overtone level show no sign of the bands from the  $3^3_4^1$ ,  $K=2$  level or the  $B^5$ ,  $K=1$  (V) level, which lie close by in our spectra taken via the  $\nu_3''$  fundamental, and have comparable intensity. One of the contributing factors must be that the composition of the two ground state levels is different, despite the similarity of their names. The  $\nu_3$  fundamental is involved in an anharmonic resonance with  $\nu_2+\nu_4+\nu_5$ , such that the eigenfunction of the  $3295\text{ cm}^{-1}$  level (which we used as the intermediate state in the present work) is an almost 50:50 mixture of the two basis functions. [23] The mixing of the two bending vibrations,  $\nu_4$  and  $\nu_5$ , into the wave function must enhance the probability of transitions to bending levels of the upper state according to the Franck-Condon principle. On the other hand the nominal  $3\nu_3$  level at  $9640\text{ cm}^{-1}$  has 62%  $\nu_3$  character and 28%  $2\nu_1+\nu_3$  character, [23] so that there is very little bending character in its eigenfunction. This phenomenon was noted in Ref. [154], where  $(1112^0_0)$  was used instead of  $3\nu_3$  as a  $J''<8$  intermediate for studying  $\nu_4'/\nu_6'$ , but this was not necessary for  $\nu_5'$  or  $3^1_5^1$ .

Contributing to the  $\nu_3''$  spectrum in this region are bands from two further states,  $B^5$ ,  $K=1$  (V) at  $46112\text{ cm}^{-1}$ , and *cis*- $6^2$ ,  $K=1$  at  $46120\text{ cm}^{-1}$ . The  $B^5$  state is unexceptional, but the *cis*- $6^2$  state is very interesting, because it provides a second example of K-staggering in the  $S_1$  electronic state caused by quantum mechanical tunnelling through the barrier to isomerization. [24] The first example of K-staggering was the *cis*- $3^1_6^1$  vibrational level, discussed in [11].

The selection rules for transitions to *cis* upper states are different from those to *trans* upper states. Bands involving even-K and odd-K rotational states of *cis* vibrational levels cannot



appear in the same spectrum because different numbers of photons are needed to record them. For an  $A_1$  vibrational level such as  $\text{cis-6}^2$ , its  $K=0$  state can be observed in one-photon hot band spectra from an  $l'' = 1g$  level such as  $\nu_4''$  ( $\pi_g$ ), but its  $K=1$  state requires IR-UV double resonance via an  $l''=0u$  level, such as  $\nu_3''$  ( $\sigma_u^+$ ). Experimentally, the  $\text{trans-1}^13^1$ ,  $K=0$  state at  $46114.5 \text{ cm}^{-1}$ , as observed in one-photon hot band spectra from  $\nu_4''$ , was found [11] to undergo an avoided crossing with the  $\text{cis-6}^2$ ,  $K=0$  state, which lies at  $46114.0 \text{ cm}^{-1}$ . The  $\text{cis-6}^2$ ,  $K=1$  state should then be observable near this energy in IR-UV double resonance spectra via  $\nu_3''$ . In this work a band with  $K'=1$ , which appears at  $46120.3 \text{ cm}^{-1}$  in IR-UV double resonance via  $\nu_3''$ , is assigned to  $\text{cis-6}^2$ . The upper state therefore has an apparent  $A-\frac{1}{2}(B+C)$  constant of  $6.3 \text{ cm}^{-1}$ . The expected value of this quantity is about  $13 \text{ cm}^{-1}$ , which suggests that the upper state  $K$ -structure exhibits an even-odd  $K$ -staggering, which is one of the results of tunnelling through the barrier to isomerization.[24] The  $\text{cis-6}^2$   $K'=0$  and  $1$  bands, as observed in a one-photon hot band from  $\nu_4''$  and in IR-UV double resonance via  $\nu_3''$ , respectively, are illustrated in Fig. 7. Both bands are overlapped by other structure.

Two  $K'=2$  states, one from  $B^5$  and the other from  $2^1B^3$ , are expected at  $46059 \text{ cm}^{-1}$ , but only one very weak band is found. It is provisionally assigned to  $B^5$ , since this polyad generally gives stronger bands than  $2^1B^3$ . Of the 43 upper states with  $K'=0-2$  expected in the  $45800 - 46250 \text{ cm}^{-1}$  region, only three have not been identified, although their positions can be predicted to within a very few  $\text{cm}^{-1}$ .

#### 4.5 The $3^2B^3$ and $2^13^2B^1$ polyads ( $46250 - 46550 \text{ cm}^{-1}$ )

The next bands in the IR-UV double resonance spectra, in order of increasing energy, lie in the region  $46250 - 46550 \text{ cm}^{-1}$ . Although the region contains only seven vibrational levels from the trans manifold, accidental overlapping of bands from two polyads,  $3^2B^3$  and  $2^13^2B^1$ , produces some surprisingly complicated structures. The other states contributing to the region are  $2^15^1$ ,  $B^5$  and the new cis levels  $3^2$  and  $4^16^1$ . Nearly all the structure from the  $B^5$  polyad lies in the regions described above, but the Darling-Dennison resonance effects in it are so large that its highest  $K'=1$  and  $2$  states are several hundred  $\text{cm}^{-1}$  above its lowest states. The highest-energy  $K' = 1$  state appears at  $46292.3 \text{ cm}^{-1}$ ,  $4 \text{ cm}^{-1}$  below its predicted [165] position, and the highest  $K' = 2$  state (not found) is predicted to lie at  $46424 \text{ cm}^{-1}$ .

Figure 8 gives an overview of the region, in the form of a stick spectrum of the  $K'=0-2$  levels. When two quanta of  $\nu_3$  are excited, the very large cross-anharmonicity between  $\nu_3$  and  $\nu_6$  starts to break up the bending polyads. Even though the two bending fundamentals,  $\nu_4$  and  $\nu_6$ , are only  $3 \text{ cm}^{-1}$  apart, [154] the result in the  $3^2B^3$  polyad is that the nominal  $3^26^3$  ( $B_u$ ) level lies  $110 \text{ cm}^{-1}$  below the nominal  $3^24^3$  ( $A_u$ ) level. The Darling-Dennison resonance pushes the combination levels  $3^24^16^2$  ( $A_u$ ) and  $3^24^26^1$  ( $B_u$ ) more than another  $100 \text{ cm}^{-1}$  higher still, so that the four  $K=0$  levels are spread over  $250 \text{ cm}^{-1}$ . The Coriolis effects are then not strong enough to

cause re-ordering of the low-K energy levels, such as is seen in the  $1^1B^1$  and  $2^1B^3$  polyads, except in the third of the four vibrational levels (in order of energy). The K-structure is more like that of a slightly perturbed asymmetric top, though the lowest  $K=0$  and 1 levels lie very close in energy, which (as we see below) can lead to interesting effects. The  $2^13^2B^1$  polyad behaves in similar fashion, except that there is no Darling-Dennison resonance. The predicted positions of the states of these polyads (following Eq. (1)) are given in **Table 2**. The agreement between the observed and calculated positions is not as good as for the  $B^5$  polyad, though it is still adequate to allow assignment of the bands.

The lowest  $K'=0$  and 1 levels of the  $3^2B^3$  polyad give rise to weak bands near  $46290\text{ cm}^{-1}$ . There is no direct coupling between them, but transferred b-axis Coriolis interaction causes both of them to appear in double resonance spectra via both  $v_3''$  and  $(v_3+v_4)''$ . The lower  $K'=0$  and 1 levels of the  $2^13^2B^1$  polyad (nominally  $2^13^26^1$ ,  $B_u$ ) lie at  $46359\text{ cm}^{-1}$ . They are almost degenerate, and since the nominal  $2^13^24^1$ ,  $A_u$ ,  $K=1$  level, to which they are both Coriolis-coupled, lies only  $28\text{ cm}^{-1}$  higher, there is strong interaction. The spectrum, as seen in double resonance via the very sharp Q branch head of  $v_3+v_4''$  ( $\Pi_u$ ), where the  $J'' = 1f - 5f$  levels are populated simultaneously by the IR laser, is illustrated in **Fig. 9**. It is unexpectedly complicated. According to the rotational selection rules, there should be two sets of R and P branches, one going to the  $K'=0f$  state, and the other to the  $f$  symmetry levels of the  $K'=1$  state as a result of the Coriolis interaction. Instead three strong R-P branch pairs are seen, together with two weak Q branches in the gap between them. This implies that three sets of excited state  $f$  symmetry rotational levels and two sets of  $e$  symmetry levels are present. Given that the unperturbed  $K'=1e$  levels may give rise to a weak Q branch if other suitable interactions occur, it is clear that an extra vibrational state must be present. The upper state energy levels are shown, plotted against  $J(J+1)$ , in **Fig. 10**. The parabola-like appearance of this figure is reminiscent of **Fig. 6**, and for the same reason. In fact the branch intensities, and the existence of a  $J'=0$  level for the middle set of  $f$  symmetry levels, show that the zero-order  $2^13^26^1$ ,  $K'=0$  and 1 states correspond to the three lowest sets of levels. The two sets of  $f$  symmetry levels,  $K'=0f$  and  $1f$ , repel each other, while the  $K'=1e$  set, which is unaffected, lies in between them. Further interactions between the  $f$  symmetry levels then transfer the curvature of the plot to the upper set of  $f$  levels in the figure. A small perturbation in the topmost  $f$  level appears to be caused by an unidentified  $K'=4$  state. The pattern of upper state energy levels is confirmed in detail by the double resonance spectrum via  $v_3''$ , where the  $f$  symmetry levels give Q branches, and the  $e$  symmetry levels give R and P branches.

There is no place in the  $S_1$ -trans manifold for the upper  $K'=1$  state, which presumably belongs to the  $S_1$ -cis manifold. *Ab initio* calculations of the cis vibrational structure [149] predict that the cis- $2^1$  and  $3^2$  levels should both lie within a very few  $\text{cm}^{-1}$  of each other close to this energy. These vibrational levels both have the correct symmetry ( $A_1$ ) to give  $K'=1$  bands in the  $v_3''$  double resonance spectrum, but the *ab initio* calculations [12] indicate that the cis- $3^2$  level should interact much more strongly than the cis- $2^1$  level with the trans manifold and have greater

intensity via  $\nu_3''$ . In view of these calculations, we provisionally assign the new  $K'=1$  state as  $\text{cis-}3^2$ .

The next region of complexity occurs about  $50\text{ cm}^{-1}$  higher, where three close-lying  $K'=1$  states occur at 46408, 46414 and  $46416\text{ cm}^{-1}$ . All three have comparatively large asymmetry splittings (see Table 1) in the sense  $f$  above  $e$ , which is consistent with  $A_u$  vibrational symmetry. Predictions of the  $K$ -rotational structures of the  $3^2B^3$  and  $2^13^2B^1$  polyads would place  $K'=1$  states with  $A_u$  symmetry at 46411 and  $46418\text{ cm}^{-1}$ , respectively. Unfortunately the predictions are not accurate enough to identify the observed states with particular polyads securely, though it seems that the states at 46414 and  $46416\text{ cm}^{-1}$ , which give the strongest bands, belong to these two polyads. However the third state, which gives a much weaker band, is not predicted, and presumably belongs to the  $S_1$ -cis electronic state, where its vibrational symmetry would be  $B_1$ . Vibrational  $B_1$  states are rare among the low-lying levels of the  $S_1$ -cis state, as they require odd quanta of both  $\nu_4$  ( $a_2$ ) and  $\nu_6$  ( $b_2$ ). At this very low vibrational energy of approximately  $1500\text{ cm}^{-1}$  the only logical assignment is the combination level  $\text{cis-}4^16^1$ .

There are only a few triplet perturbations in this region. Most of them take the form of a doubling of the  $J'=K'$  lines of a band, but more extensive perturbations occur in the  $3^2B^3$ ,  $K=1$  (IV) state at  $46598\text{ cm}^{-1}$ , where several  $J$  levels are affected; the  $J=5e$  level of this state is split into four components. Where the vibrational assignments of the perturbed states have been established, it is found that they all belong to the  $3^2B^3$  polyad.

The  $2^15^1$  vibrational level lies in the middle of this region, at  $46441\text{ cm}^{-1}$ , and has been observed previously. [25] It is not subject to Coriolis effects, and is a "normal" asymmetric top level. Our rotational constants for it are given in Table 3.

## 5. Discussion

This work gives the details of the *ungerade* vibrational levels of the  $S_1$ -trans state of acetylene in the energy range  $45800 - 46500\text{ cm}^{-1}$ , as observed in IR-UV double resonance. The complete vibrational level structure of this electronic state has now been established up to a vibrational energy of  $4300\text{ cm}^{-1}$ . The aim has been to understand the  $S_1$ -trans state in sufficient detail that any vibrational states that do not fit into its energy level pattern can be assigned to the  $S_1$ -cis isomer. Four such states were identified previously, [11] and the present work has provisionally found two more.

The barrier to isomerization in the  $S_1$  state is calculated [12] to lie around  $5000\text{ cm}^{-1}$  above the  $S_1$ -trans zero-point level, which means that the signatures of cis-trans isomerization should already be observable in some of the levels studied in this work. The most characteristic effect will be an even-odd staggering in the  $K$ -structure of a vibrational level where tunnelling through the barrier is possible. [24] This effect should be largest in those vibrational levels that

carry the shape of the molecule along the isomerization pathway from the equilibrium structure of the trans isomer to the half-linear structure at the saddle point. Those vibrational levels are combinations of  $\nu_3$  and  $\nu_6$ , which in the trans isomer are, respectively, the trans-bend and the cis-bend. (The forms of the vibrations are reversed in the cis isomer.) It is difficult to observe the K-staggering in levels of the trans isomer because the Coriolis and Darling-Dennison interactions between  $\nu_6$  and  $\nu_4$  (torsion) perturb the K-rotational structure so severely that the effects of the tunnelling are masked. The interaction between  $\nu_4$  and  $\nu_6$  is less important in the cis isomer, so that the K-staggering can be observed. The cis- $3^16^1$  level was recently found [11] to have its  $K'=1$  state shifted up by  $3.9\text{ cm}^{-1}$  relative to its  $K'=0$  and 2 states. From the present work, the cis- $6^2$  level appears to have a staggering of about  $7\text{ cm}^{-1}$  in the opposite sense.

Nevertheless, trans-levels in the same energy region as these cis levels should show comparable staggerings, and the  $3^2B^3$  polyad, in the region  $46250 - 46550\text{ cm}^{-1}$ , should offer good examples. It may be that hints of their existence can already be seen. It was found [16] that the vibrational and K-rotational structures of the pure bending polyads,  $B^n$ ,  $n=1-3$ , can all be reproduced to within a very few  $\text{cm}^{-1}$  by a single set of anharmonicity and interaction parameters; the present work confirms that this finding applies also to the states of the  $B^5$  polyad. A similar finding applies to the various bending polyads in combination with symmetric levels such as  $3^1$ , and forms the basis for extending the vibrational assignments to higher energy.[10] On the other hand, this approach works less well for predicting the structure of the  $3^2B^3$  polyad, perhaps indicating that staggerings are present, but are less completely masked by the intrapolyad interactions. It will be interesting to follow the level patterns to higher energies, where the bending polyad structure is essentially destroyed by the anharmonicity, so that the effects of the barrier should be more clearly seen.

Now that the structures of the trans polyads in this region have been established, it should be possible to analyze the region near the expected transition state energy, located approximately one bending quantum higher. The information gained from the present analysis of the  $1^1B^1$  and  $2^1B^3$  polyads has already helped with the analysis of that energy region in our not yet published one-photon spectra, which contain candidates for additional cis levels and the barrier-proximal levels  $3^36^2$  and  $3^46^2$ . The analysis of these levels, and the information about the transition state energy that can be derived from it, will be discussed in a future paper.

### Acknowledgements

This work was supported at MIT by (U.S.) Department of Energy (DOE) Grant No. DE-FG0287ER13671. PBC acknowledges support from the MIT Undergraduate Research Opportunities Program. AJM thanks Academia Sinica, Taiwan, for financial support and the University of British Columbia for some travel funding.

## References

- [1] G.W. King and C.K. Ingold, *Nature (London)* **169**, 1101 (1952).
- [2] C.K. Ingold and G.W. King, *J. Chem. Soc.* **1953**, 2702.
- [3] K.K. Innes, *J. Chem. Phys.* **22**, 863 (1954).
- [4] J.F. Stanton, C.M. Huang and P.G. Szalay, *J. Chem. Phys.* **101**, 356 (1994).
- [5] Q. Cui, K. Morokuma and J.F. Stanton, *Chem. Phys. Lett.* **263**, 46 (1996).
- [6] Q. Cui and K. Morokuma, *Chem. Phys. Lett.* **272**, 319 (1997).
- [7] K. Malsch, R. Rebentisch, P. Swiderek and G. Hohlneicher, *Theor. Chem. Acc.* **100**, 171 (1998).
- [8] E. Ventura, M. Dallos and H. Lischka, *J. Chem. Phys.* **118**, 1702 (2003).
- [9] H. Köppel, B. Schubert and H. Lischka, *Chem. Phys.* **343**, 319 (2008).
- [10] A.H. Steeves, H.A. Bechtel, A.J. Merer, N. Yamakita, S. Tsuchiya and R.W. Field, *J. Mol. Spectrosc.* **256**, 256 (2009).
- [11] A.J. Merer, A.H. Steeves, J.H. Baraban, H.A. Bechtel and R.W. Field, *J. Chem. Phys.* **134**, 244310 (2011).
- [12] J.H. Baraban, A.R. Beck, A.H. Steeves, J.F. Stanton and R.W. Field, *J. Chem. Phys.* **134**, 244311 (2011).
- [13] M. Mizoguchi, N. Yamakita, S. Tsuchiya, A. Iwasaki, K. Hoshina and K. Yamanouchi, *J. Phys. Chem. A* **104**, 10212 (2000).
- [14] J.H. Baraban, J.F. Stanton, A.J. Merer and R.W. Field, *Mol. Phys.*, submitted [to appear in the same issue as the present paper].
- [15] A.L. Utz, J.D. Tobiason, E. Carrasquillo M., L.J. Sanders and F.F. Crim, *J. Chem. Phys.* **98**, 2742 (1993).
- [16] A.J. Merer, N. Yamakita, S. Tsuchiya, A.H. Steeves, H.A. Bechtel and R.W. Field, *J. Chem. Phys.* **129**, 054304 (2008).
- [17] J.K.G. Watson, M. Herman, J.C. Van Craen and R. Colin, *J. Mol. Spectrosc.* **95**, 101 (1982).
- [18] J.C. Van Craen, M. Herman, R. Colin and J.K.G. Watson, *J. Mol. Spectrosc.* **111**, 185 (1985).
- [19] J.D. Tobiason, A.L. Utz and F.F. Crim, *J. Chem. Phys.* **99**, 928 (1993).
- [20] W.J. Lafferty and A.S. Pine, *J. Mol. Spectrosc.* **141**, 223 (1990).
- [21] N. Yamakita and S. Tsuchiya, *Chem. Phys. Lett.*, **348**, 53 (2001).
- [22] K. L. Bittinger. *Spectroscopic Signatures of Doorway-Mediated Intersystem Crossing*. PhD thesis, Massachusetts Institute of Technology, 2009.
- [23] M. Herman, J. Liévin, J. Vander Auwera and A. Campargue, *Adv. Chem. Phys.* **108**, 1 (1999).
- [24] J.T. Hougen and A.J. Merer, *J. Mol. Spectrosc.* **267**, 200 (2011).

Formatted: Left, Level 1

[25] M.A. Payne, A.P. Milce, M.J. Frost, and B.J. Orr. Chem. Phys. Lett. **324**, 48 (2000).

For Peer Review Only

### Captions for figures

Fig. 1. Stick diagram of the *ungerade*  $K'=0-2$  levels of the  $\tilde{A}^1A_u$  ( $S_1$ -trans) state of  $C_2H_2$  in the region  $45800 - 46240\text{ cm}^{-1}$ , with their assignments, as recorded using IR-UV double resonance via the  $\nu_3''$  ( $\sigma_u^+$ ) and  $(\nu_3+\nu_4)''$  ( $\Pi_u$ ) vibrational levels of the ground state. The two spectra have been combined into a single plot. States that could not be found are marked with dotted lines at their predicted positions. Two vibrational levels of the  $\tilde{A}^1A_2$  ( $S_1$ -cis) state also appear; their positions are indicated with dashed lines.

Fig. 2. Observed energy level structure of the ten states with  $K'=0-2$  from the  $2^1B^3$  and  $1^1B^1$  polyads in the region  $45800 - 45840\text{ cm}^{-1}$ . The  $K'$ -assignments are given in two columns,  $1^1B^1$  on the left and  $2^1B^3$  on the right. Rotational levels of  $e$  symmetry are shown with open circles and dashed lines; those of  $f$  symmetry are shown with full circles and solid lines. In the online version, levels of  $e$  symmetry are coloured red, and levels of  $f$  symmetry are coloured blue. A strong B-axis Coriolis interaction occurs between the upper  $K'=1$  and  $2$  states of the  $2^1B^3$  polyad. The  $2^1B^3$  state ( $K=0$ ,  $Bb_u$ ) lies  $0.2\text{ cm}^{-1}$  above the  $2^1B^3$  state ( $K=0$ ,  $Aa_u$ ), and has an essentially identical B value.

Fig. 3. IR-UV double resonance spectrum of  $C_2H_2$  in the region  $45820 - 45850\text{ cm}^{-1}$ , as observed via levels of the  $\nu_3''$  ( $\sigma_u^+$ ) fundamental of the ground state. Five spectra (from  $J''=0-4$ ) are plotted on top of each other, to give the appearance of a single spectrum. Six bands are shown; they are named according to the energies of their band origins in  $\text{cm}^{-1}$ , as in Fig. 2. Their J assignments are each given on a single horizontal tie-line, except for the  $45838\text{ cm}^{-1}$   $K'=1$  band, which is shown on two lines; it has an unusual structure where the R branch forms a head at  $J=1$ . The energy scale is that of the UV laser.

Fig. 4. IR-UV double resonance spectra of  $C_2H_2$  showing the  $\tilde{A}^1A_u$ ,  $3^3B^1$ ,  $K'=1$  band as seen via the  $J''=0-5$  levels of the ground state  $\nu_3''$  ( $\sigma_u^+$ ) vibrational level at  $3295\text{ cm}^{-1}$ . The  $J'=2$  patterns are indicated by tie-lines in all three branches to indicate the position of the principal perturbing  $K'=2$  state. Some rotational lines marked Q and R belong to the  $K'=3$  state that interacts with the perturbing  $K'=2$  state, causing its energy level pattern to be distorted. For clarity, some Q lines from the  $3^3B^1$ ,  $K'=0$  band and some R lines from the  $B^5$ ,  $K'=1$  (II) band are shown ~~dashed~~~~dotted~~. The energy scale is that of the UV laser.

Fig. 5. Energy levels of the  $\tilde{A}^1A_u$ ,  $3^3B^1$ ,  $K'=1$  state of  $C_2H_2$ , plotted against  $J(J+1)$ . Levels of  $e$  symmetry are shown as squares, and levels of  $f$  symmetry are shown as circles. In the online version, levels of  $e$  symmetry are coloured red, and levels of  $f$  symmetry are coloured blue. The sizes of the symbols roughly represent the intensities of the lines in Fig. 4. The  $3^3B^1$ ,  $K'=1$  state interacts with the  $B^5$ ,  $K=2$  (II) state and (more weakly) with a number of "background" triplet levels. A third set of energy levels (~~dashed~~~~dotted~~ line) is assigned to the  $2^2B^1$ ,  $K=4$  (II) state. The S-shaped pattern of the upper set of levels should be noted; it arises from strong Coriolis coupling between the  $B^5$ ,  $K=2$  (II) and  $B^5$ ,  $K=3$  (I) states, as illustrated in Fig. 6.



Fig. 6. Observed and calculated energy levels of the  $\tilde{A}^1A_u$ ,  $B^5$  polyad of  $C_2H_2$  in the neighbourhood of the  $3^36^1$ ,  $K=1$  state, plotted against  $J(J+1)$ . Observed levels are shown as full circles joined by solid lines; calculated levels are shown with open circles joined by dashed lines. In the online version, observed levels are also coloured red, and calculated levels are also coloured blue; the zero-order position of the  $3^36^1$ ,  $K=1$  state is shown in green. The calculations are based on the parameters of [165], with an offset of  $3\text{ cm}^{-1}$  added. The  $3^36^1$ ,  $K=0$  state lies at  $45937\text{ cm}^{-1}$ , but is not shown.

Fig. 7. Upper spectrum: the interacting  $cis\text{-}6^2$ ,  $K=0$  and  $trans\text{-}1^13^1$ ,  $K=0$  states, as seen in one-photon hot band spectra via the  $\nu_4''$  ( $\pi_g$ ) fundamental. These two states lie less than  $1\text{ cm}^{-1}$  apart, and are linked in the figure with a single set of tie-lines for each  $J$  value. The calibration for this spectrum is not exact; a small correction equal to  $[B(\nu_4'') - B(\nu''=0)] J''(J''+1)$  should be applied for each line. Lower spectrum: the  $cis\text{-}6^2$ ,  $K=1$  state, as seen in IR-UV double resonance via the  $\nu_3''$  ( $\sigma_u^+$ ) fundamental. This spectrum consists of five superimposed plots taken via the rotational levels  $J'' = 0\text{--}4$  individually. No correction needs to be applied to the calibration of this spectrum. The tie-lines for the  $cis\text{-}6^2$ ,  $Q(1)$  lines in the two spectra of this figure are shown thickened, in order to emphasise that the  $K'=1$  state lies only  $6.3\text{ cm}^{-1}$  above the  $K'=0$  state. This quantity corresponds to the rotational constant  $A - \frac{1}{2}(B+C)$ , less the amount of the  $K$ -staggering which results from quantum mechanical tunnelling through the barrier to isomerisation. Since  $A - \frac{1}{2}(B+C)$  is expected to be about  $13\text{ cm}^{-1}$ , the  $K$ -staggering has lowered the  $K'=1$  state, relative to the  $K'=0$  state, by about  $7\text{ cm}^{-1}$ .

Fig. 8. Stick diagram of the *ungerade*  $K' = 0\text{--}2$  levels of the  $\tilde{A}^1A_u$  state of  $C_2H_2$  in the region  $46280\text{--}46550\text{ cm}^{-1}$ , with their assignments, as recorded using IR-UV double resonance via the  $\nu_3''$  ( $\sigma_u^+$ ) and  $(\nu_3 + \nu_4)''$  ( $\Pi_u$ ) vibrational levels of the ground state. The spectra recorded from the two intermediate levels have been combined into a single plot. Approximate intensities are indicated by the heights of the sticks. States that could not be found are marked with dotted lines at their predicted positions. The highest  $K'=1$  and  $2$  states of the  $3^2B^3$  polyad are not shown; bands at  $46598.5$  and  $46696.3\text{ cm}^{-1}$  are provisionally assigned to them.

Fig. 9. IR-UV double resonance spectrum of  $C_2H_2$  near  $46359\text{ cm}^{-1}$ , recorded via the  $Q$  branch of the  $\nu_3 + \nu_4''$  ( $\Pi_u$ ) combination level. The three sets of  $R$  and  $P$  branches represent the  $K'=0f$  and  $1f$  levels of the  $2^13^26^1$  state, which are almost degenerate, together with the  $f$  levels of another  $K'=1$  state at  $46361.3\text{ cm}^{-1}$ , which is assigned as  $cis\text{-}3^2$ . All three sets of  $f$  levels are strongly Coriolis-coupled. The two  $Q$  branches represent the unperturbed  $e$  symmetry levels of the two  $K'=1$  states. In the online version, lines going to the  $cis\text{-}3^2$  state are marked in red, and lines going to the  $2^13^26^1$  state are marked in blue.

Fig. 10. Observed energy levels in the  $46359\text{ cm}^{-1}$  region of the *ungerade* manifold of the  $S_1$  state of  $C_2H_2$ , plotted against  $J(J+1)$ . The three lowest levels (two of  $f$  symmetry and one of  $e$  symmetry) belong to the  $S_1\text{-trans } 2^13^2B^1$ ,  $K=0f$  and  $1$  states, which are almost degenerate in zero-order and interact by indirect  $B$ -axis Coriolis coupling. The state near  $46361\text{ cm}^{-1}$  is assigned as



1  
2  
3  
4  
5  
6  
7  
8  
9  
10  
11  
12  
13  
14  
15  
16  
17  
18  
19  
20  
21  
22  
23  
24  
25  
26  
27  
28  
29  
30  
31  
32  
33  
34  
35  
36  
37  
38  
39  
40  
41  
42  
43  
44  
45  
46  
47  
48  
49  
50  
51  
52  
53  
54  
55  
56  
57  
58  
59  
60

cis-3<sup>2</sup>, K'=1, perturbed at J' ≥ 4 by an unidentified state. In the online version, levels of *e* symmetry are coloured red, and levels of *f* symmetry are coloured blue.

For Peer Review Only

Table 1. C<sub>2</sub>H<sub>2</sub>, band-by-band analyses of the *ungerade* states in the 45800 – 46500 cm<sup>-1</sup> region. Rotational constants (cm<sup>-1</sup>) are from least squares fittings where a r.m.s. error is given.  $q$  is the same as  $\frac{1}{2}(B-C)$  for K=1 states, and is the coefficient of  $J^2(J+1)^2$  in the asymmetry splitting of K=2 states; a positive value of  $q$  means  $e$  levels above  $f$ . D terms are needed where b-axis Coriolis coupling distorts the rotational structure of a state; these D constants do not represent true centrifugal distortion.

	K	T <sub>0</sub> <sup>(a)</sup>	3σ	B	3σ	10 <sup>2</sup> q	3σ	D	r.m.s.
2 <sup>1</sup> B <sup>3</sup>	1 (I)	45805.09 ± 0.05		0.9353 ± 0.0094		1.13 ± 0.17		(-1.60 ± 0.44) × 10 <sup>-3</sup>	0.019 <sup>(ba)</sup>
2 <sup>1</sup> 4 <sup>3</sup>	0, <u>A</u> <sub>a</sub> <sub>u</sub>	45810.66	0.08	1.1335	0.0126			(0.95 ± 0.38) × 10 <sup>-3</sup>	0.023
2 <sup>1</sup> 6 <sup>3</sup>	0, <u>B</u> <sub>b</sub> <sub>u</sub>	45810.86	0.10	1.1250	0.0096			(0.75 ± 0.16) × 10 <sup>-3</sup>	0.040
1 <sup>1</sup> B <sup>1</sup>	1 (I)	45822.99	0.17	0.9328	0.0304	-4.16	1.20	(-1.6 ± 1.0) × 10 <sup>-3</sup>	0.071
2 <sup>1</sup> B <sup>3</sup>	2 (I)	45823.07	0.18	1.1031	0.0213	0.095	0.091	(0.79 ± 0.70) × 10 <sup>-3</sup>	0.036
1 <sup>1</sup> 4 <sup>1</sup>	0, <u>A</u> <sub>a</sub> <sub>u</sub>	45825.88	0.18	1.1926	0.0294			(0.30 ± 0.09) × 10 <sup>-2</sup>	0.053
1 <sup>1</sup> 6 <sup>1</sup>	0, <u>B</u> <sub>b</sub> <sub>u</sub>	45834.26	0.08	1.1191	0.0092			(0.95 ± 0.21) × 10 <sup>-3</sup>	0.026
1 <sup>1</sup> B <sup>1</sup>	2 (I)	45838.81	0.07	1.0666	0.0067	0.094	0.032		0.018
2 <sup>1</sup> B <sup>3</sup>	1 (II)	45839.12	0.21	0.613	0.037 <sup>(cb)</sup>	0.32	1.45	(-2.4 ± 1.2) × 10 <sup>-3</sup>	0.085
2 <sup>1</sup> B <sup>3</sup>	2 (II)	45842				See Fig. 2			
1 <sup>1</sup> B <sup>1</sup>	1 (II)	45859.53	0.03	1.1053	0.0058	1.03	0.23	(0.11 ± 0.20) × 10 <sup>-3</sup>	0.013
2 <sup>1</sup> B <sup>3</sup>	1 (III)	45863.90	0.14	1.1690	0.0223	0.99	0.77	(0.37 ± 0.73) × 10 <sup>-3</sup>	0.045
B <sup>5</sup>	0, <u>B</u> <sub>b</sub> <sub>u</sub> (I)	45890.08	0.03	1.0452	0.0007				0.016
2 <sup>1</sup> B <sup>3</sup>	2 (III)	45895.39	0.07	0.9933	0.0095	-0.29	0.64	(-0.56 ± 0.26) × 10 <sup>-3</sup>	0.015
B <sup>5</sup>	1 (I)	45895.80 <sup>(de)</sup>	0.04	1.1028	0.0044	-0.81	0.19	(0.32 ± 0.10) × 10 <sup>-3</sup>	0.011
2 <sup>1</sup> B <sup>3</sup>	0, <u>A</u> <sub>a</sub> <sub>u</sub> (II)	45902.93	0.03	1.0733	0.0039				0.009
2 <sup>1</sup> B <sup>3</sup>	0, <u>B</u> <sub>b</sub> <sub>u</sub> (II)	45906.07	0.08	1.1296	0.0153			(0.65 ± 0.45) × 10 <sup>-3</sup>	0.022
1 <sup>1</sup> B <sup>1</sup>	2 (II)	45912.50	0.15	1.0923	0.0202	-0.016	0.014	(0.93 ± 0.55) × 10 <sup>-3</sup>	0.032
B <sup>5</sup>	2 (I)	45915.11	0.10	1.0005	0.0138	-0.014	0.009	(-0.58 ± 0.37) × 10 <sup>-3</sup>	0.022
B <sup>5</sup>	0, <u>A</u> <sub>a</sub> <sub>u</sub> (II)	45919.28	0.10	1.0991	0.0061				0.046
B <sup>5</sup>	1 (II)	45931.17	0.023	0.9963	0.0033	-1.87	0.19	(0.31 ± 0.09) × 10 <sup>-3</sup>	0.010
3 <sup>3</sup> 6 <sup>1</sup>	0, <u>B</u> <sub>b</sub> <sub>u</sub>	45937.76	0.02	1.0476	0.0006				0.006
B <sup>5</sup>	2 (II)	45942				See Fig. 5			

1  
2  
3  
4  
5  
6  
7  
8  
9  
10  
11  
12  
13  
14  
15  
16  
17  
18  
19  
20  
21  
22  
23  
24  
25  
26  
27  
28  
29  
30  
31  
32  
33  
34  
35  
36  
37  
38  
39  
40  
41  
42  
43  
44  
45  
46  
47  
48  
49

	$3^3 6^1$	1	45945					See Fig. 5	
	$2^1 B^3$	1 (IV)	45969.09	0.06	1.0846	0.0100	0.42	0.40	$(0.43 \pm 0.34) \times 10^{-3}$
	$3^3 6^1$	2	45972.24	0.05	1.0703	0.0014	-0.0018	0.0027	0.030
	$B^5$	1 (III)	45983.006	0.031	1.0786	0.0057	2.18	0.35	$(-0.08 \pm 0.19) \times 10^{-3}$
	$B^5$	0, $\underline{B}b_u$ (III)	46007.5 <sub>8</sub>		1.13			only two rotational levels	
	$3^3 4^1$	0, $\underline{A}a_u$	46016.36	0.06	1.0863	0.0025			0.028
	$B^5$	0, $\underline{A}a_u$ (IV)	46022.34	0.02	1.1218	0.0012			0.009
	$3^3 4^1$	1	46040.17	0.05	1.0836	0.0021	-4.83	0.22	0.023
	$B^5$ , K=2	(IV)	46058.6 <sup>(ed)</sup>		1.057		0.04	very weak band	
	$3^1 5^1$	0, $\underline{B}b_u$	46091.75	0.07	1.0743	0.0060			0.027
	$3^1 5^1$	1	46104.31	0.04	1.0695	0.0022	4.35	0.26	0.016
	$3^3 4^1$	2	46104.7 <sub>8</sub>	0.15	1.0793	0.0065	0.060	0.014	perturbed
	$B^5$	1 (V)	46112.44	0.026	1.1645	0.0019	0.25	0.25	0.015
	cis-6 <sup>2</sup>	1	46120.338	0.018	1.0845	0.0013	5.02	0.15	0.010
	$3^1 5^1$	2	46141.91	0.03	1.0750	0.0009	-0.0024	0.0014	0.020
	$B^5$	2 (V)	46169.68	0.05	1.0906	0.0021	-0.0025	0.0063	0.019
	$B^5$	0, $\underline{B}b_u$ (V)	46190.69	0.01	1.1252	0.0004			0.005
	$B^5$	0, $\underline{A}a_u$ (VI)	46191.01	0.02	1.1256	0.0010			0.007
	$3^2 B^3$	0, $\underline{B}b_u$ (I)	46287.045	0.066	1.0336	0.0023			0.018
	$3^2 B^3$	1 (I)	46290.995	0.019	1.0808	0.0013	-0.38	0.16	0.010
	$B^5$	1 (VI)	46292.29		1.113		0	Only three rotational levels	
	$3^2 B^3$	2 (I)	46321.686	0.023	1.0423	0.0006	-0.002	0.001	0.011
	$2^1 3^2 B^1$	1e (I) <sup>(fe)</sup>	46358.80	0.13	1.050	0.008		See Fig. 10	0.058
	$2^1 3^2 B^1$	0, $\underline{B}b_u$	46359.3					See Fig. 10	
	cis-3 <sup>2</sup>	1	46361.2 <sub>8</sub>		1.07 <sub>9</sub>		-0.041	See Fig. 10	
	$2^1 3^2 B^1$	2 (I)	46380.339	0.068	1.0725	0.0054	-0.035	0.003	$(0.10 \pm 0.08) \times 10^{-3}$
	$2^1 3^2 B^1$	0, $\underline{A}a_u$	46386.95	0.08	1.0977	0.0047			0.035
	$3^2 B^3$	0, $\underline{A}a_u$ (II)	46397.83	0.07	1.0734	0.0023			0.037
	cis-4 <sup>1</sup> 6 <sup>1</sup>	1	46407.702	0.036	1.0602	0.0025	-3.32	0.30	0.018

$3^2B^3$	1 (II)	46413.84	0.02	1.0751	0.0010	-3.33	0.12	0.013
$2^13^2B^1$	1 (II)	46415.82	0.02	1.0677	0.0011	-4.13	0.14	0.013
$3^2B^3$	2 (II)	46430.07	0.08	1.0063	0.0039	-0.027	0.018	0.039
$2^13^2B^1$	2 (II)	46476.107	0.029	1.0725	0.0006	-0.0019	0.0008	0.021
$3^2B^3$	1 (III)	46479.619	0.026	1.0484	0.0045	1.24	0.74	0.013
$3^2B^3$	2 (III)	46500.817	0.037	1.1305	0.0039		$(0.45 \pm 0.08) \times 10^{-3}$	0.010
$3^2B^3$	0, $\underline{Bb}_u$ (III) <sup>(gf)</sup>	46510.969	0.070	1.1193	0.0046		$(-0.10 \pm 0.08) \times 10^{-4}$	0.025
$3^2B^3$	0, $\underline{Aa}_u$ (IV) <sup>(hg)</sup>	46541.93	0.06	1.028	0.008			0.018
$3^2B^3$	1 (IV)	46598.4 <sub>8</sub>		1.090			perturbed	
$3^2B^3$	2 (IV)	46696.267	0.012	1.0846	0.0004			0.007

(a) The electronic origin of the transition ( $T_{00}$ ) lies at  $42197.57 \text{ cm}^{-1}$ . [17]

(ba)  $H = (-0.125 \pm 0.054) \times 10^{-4}$

(cb) Very strong Coriolis interaction with  $2^1B^3$ ,  $K=2$  (II).

(de)  $J=1$  levels omitted from the fit.

(ed) Only four levels;  $J$ -assignments not secure. Two  $K=2$  levels predicted at this position:  $B^5$ ,  $K=2$  (IV) and  $2^1B^3$ ,  $K=2$  (IV); assigned to  $B^5$  on the basis of intensity.

(fe) No attempt has been made to fit the various levels of the  $46359 \text{ cm}^{-1}$  group, except for the  $K=1e$  levels of  $2^13^2B^1$ . See text for further details.

(gf) This state is perturbed, but it is not easy to pick out the avoided crossings. Many of the states at this energy suffer from triplet perturbations.

(hg) The vibrational assignment of this state is not definite, since it lies further from the expected position than the other bands in the polyad (See Table 2). An assignment of  $5^1B^2$  is also possible.

Formatted: Font color: Red

1  
2  
3  
4  
5  
6  
7  
8  
9  
10  
11  
12  
13  
14  
15  
16  
17  
18  
19  
20  
21  
22  
23  
24  
25  
26  
27  
28  
29  
30  
31  
32  
33  
34  
35  
36  
37  
38  
39  
40  
41  
42  
43  
44  
45  
46  
47  
48  
49  
50  
51  
52  
53  
54  
55  
56  
57  
58  
59  
60

Table 2. Observed and predicted level energies (cm<sup>-1</sup>) for the 3<sup>2</sup>B<sup>3</sup> and 2<sup>1</sup>3<sup>2</sup>B<sup>1</sup> polyads. Observed band energies are in Roman type, predicted energies in italic type.

	K=0	1	2
3 <sup>2</sup> B <sup>3</sup> <del>Bb<sub>u</sub></del>	46287.0	46291.0	46321.7
	<i>46291.9</i>	<i>46298.6</i>	<i>46319.6</i>
<del>Aa<sub>u</sub></del>	46397.8	46413.8	46430.1
	<i>46399.7</i>	<i>46411.3</i>	<i>46430.9</i>
<del>Bb<sub>u</sub></del>	46511.0	46479.6	46500.8
	<i>46512.9</i>	<i>46483.4</i>	<i>46498.6</i>
<del>Aa<sub>u</sub></del>	46541.9 <sup>(a)</sup>	46598.5	46696.3 <sup>(b)</sup>
	<i>46532.3</i>	<i>46595.2</i>	<i>46694.9</i>
2 <sup>1</sup> 3 <sup>2</sup> B <sup>1</sup> <del>Bb<sub>u</sub></del>	~46359 <sup>(c)</sup>	46358.8	46380.3
	<i>46356.3</i>	<i>46359.8</i>	<i>46380.4</i>
<del>Aa<sub>u</sub></del>	46387.0	46415.8	46476.1
	<i>46395.6</i>	<i>46418.1</i>	<i>46475.1</i>

- (a) The vibrational assignment of this state is not definite, since it lies further from the expected position than the other bands in the polyad. An assignment of 5<sup>1</sup>B<sup>2</sup> is also possible.
- (b) Assignment not secure. An alternative assignment to a K=2 state at 46707.7 cm<sup>-1</sup> is possible.
- (c) ~~Assumed to be the K=0 state in the 46359 cm<sup>-1</sup> group.~~ See text [and Fig. 10](#) for further details.

Table 3. Rotational constants from least squares fitting of the K'=0–2 levels of the 2<sup>1</sup>5<sup>1</sup> vibrational state. Values in cm<sup>-1</sup>.

T <sub>0</sub>	46440.894	± 0.028
A	12.587	0.041
B	1.1150	0.0039
C	1.0206	0.0040
rms	0.016	

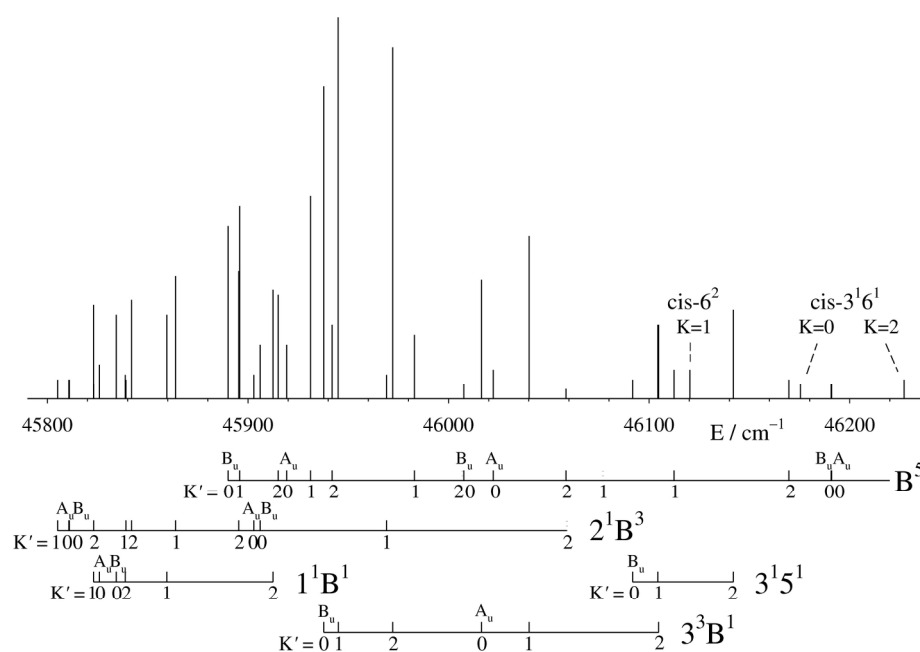


Figure 1 BW  
190x142mm (300 x 300 DPI)

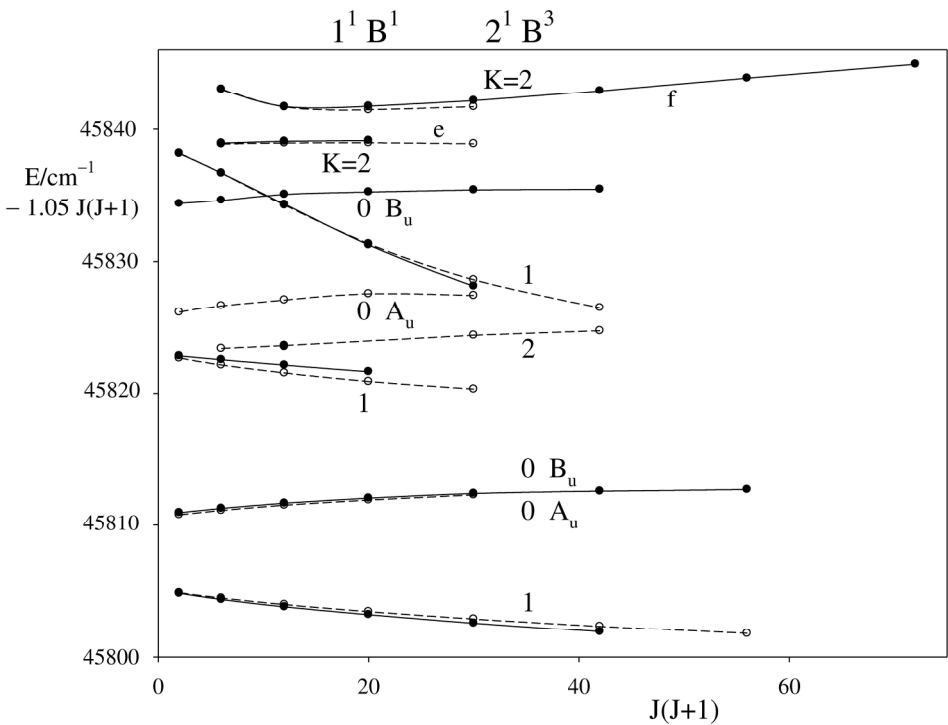


Figure 2 BW  
190x142mm (300 x 300 DPI)

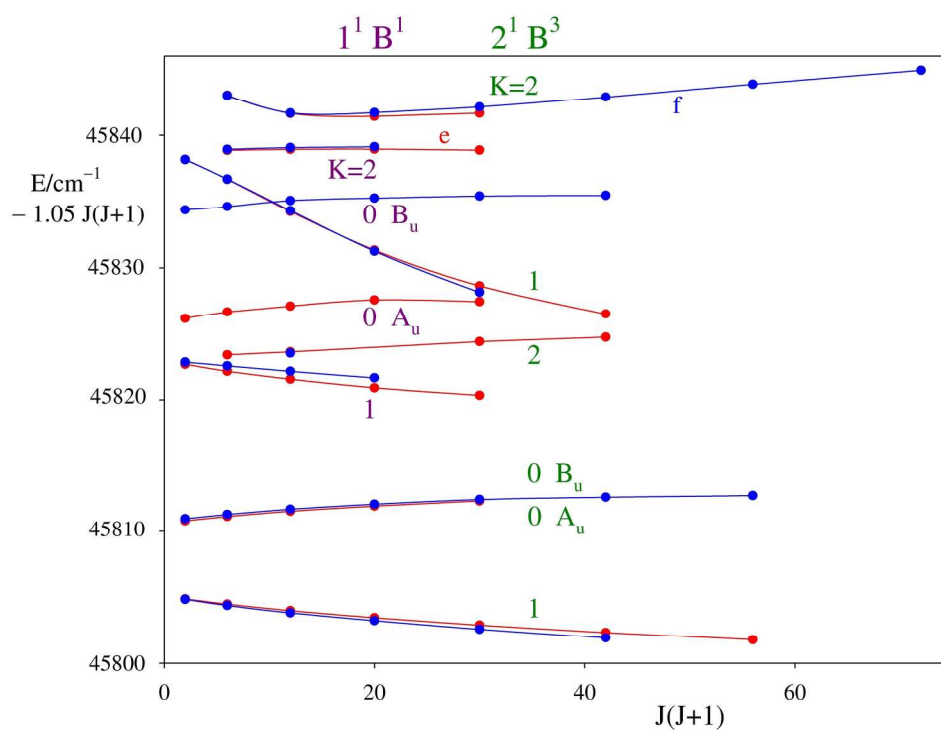
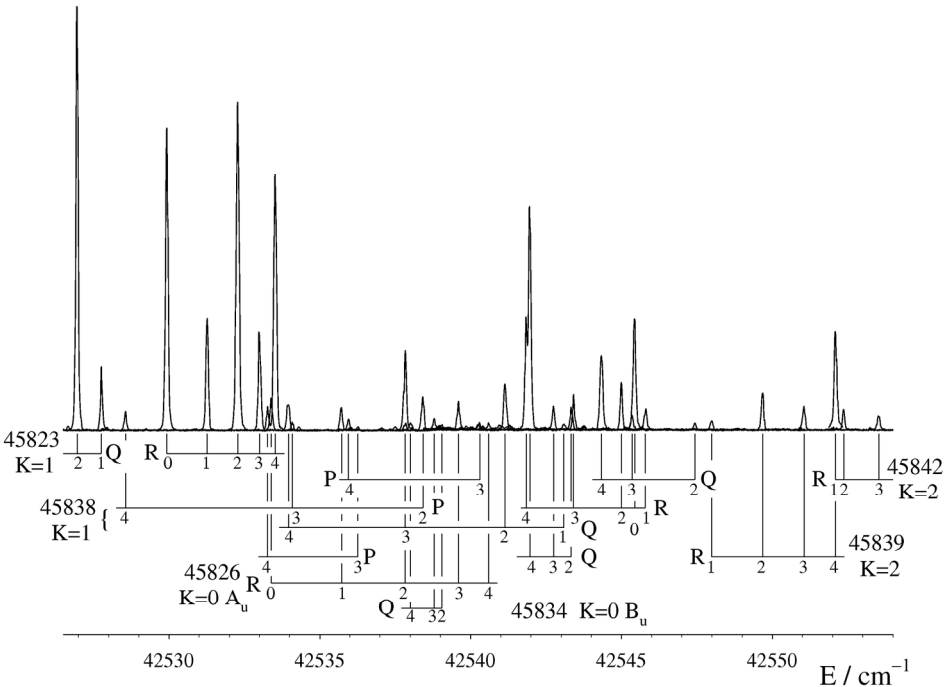
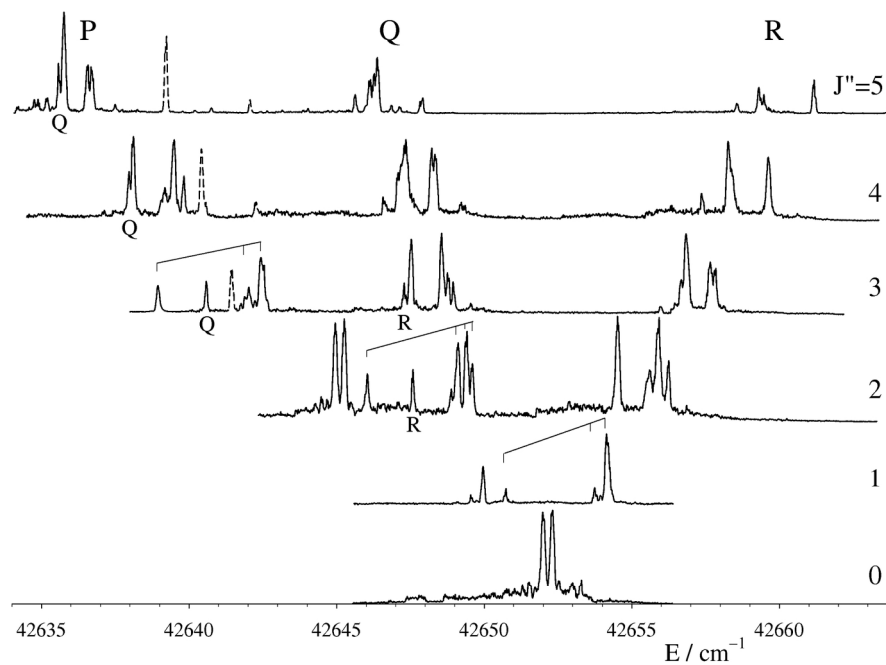


Figure 2 Color  
190x142mm (300 x 300 DPI)

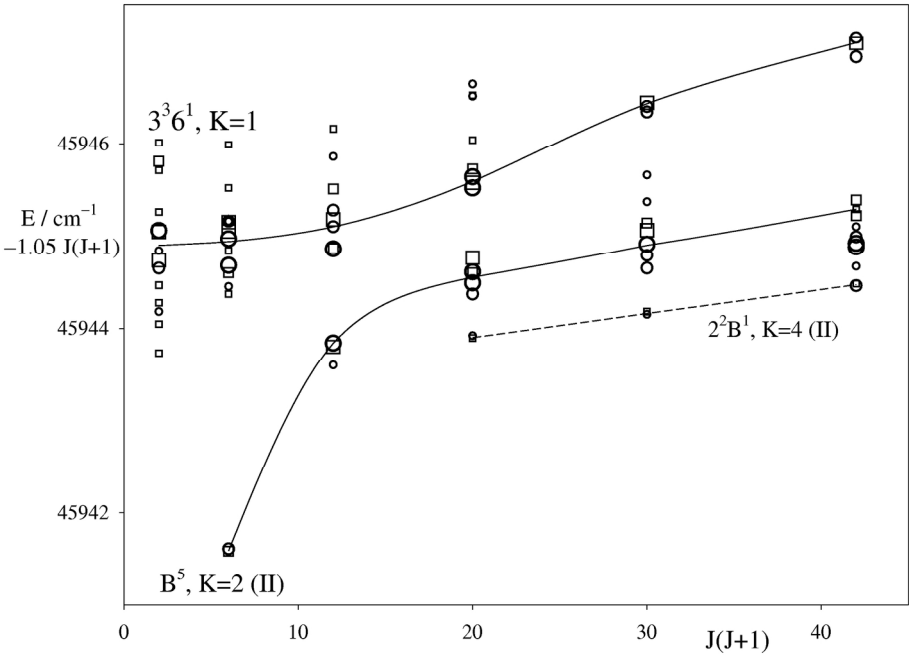




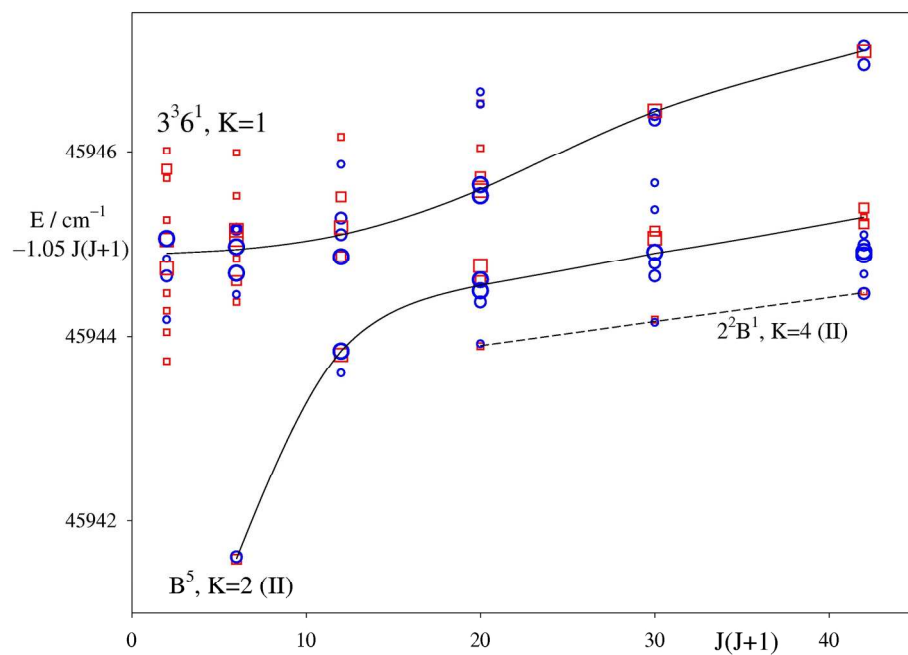
190x142mm (300 x 300 DPI)



190x142mm (300 x 300 DPI)



190x142mm (300 x 300 DPI)



190x142mm (300 x 300 DPI)

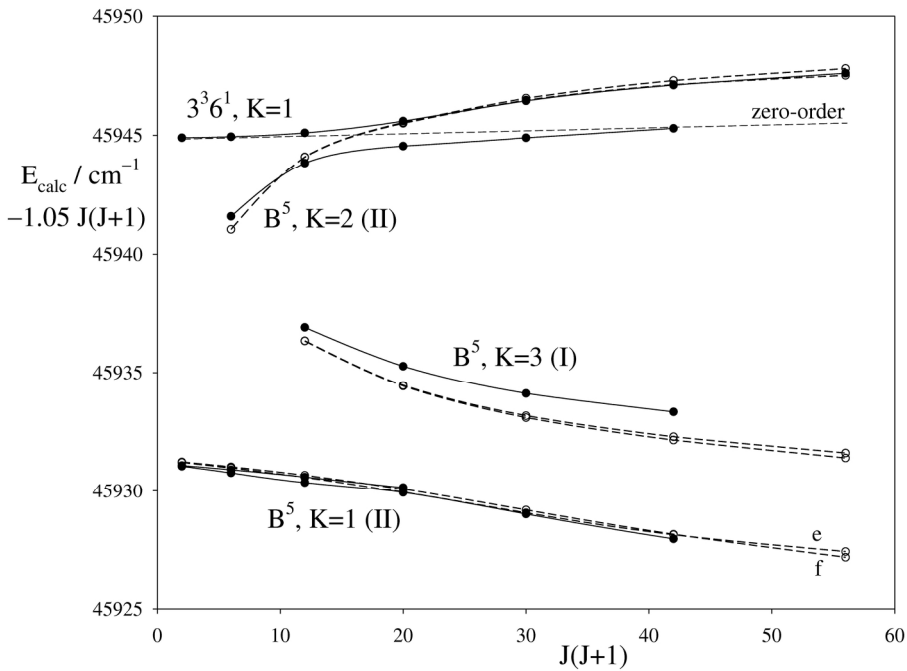


Figure 6 BW  
190x142mm (300 x 300 DPI)

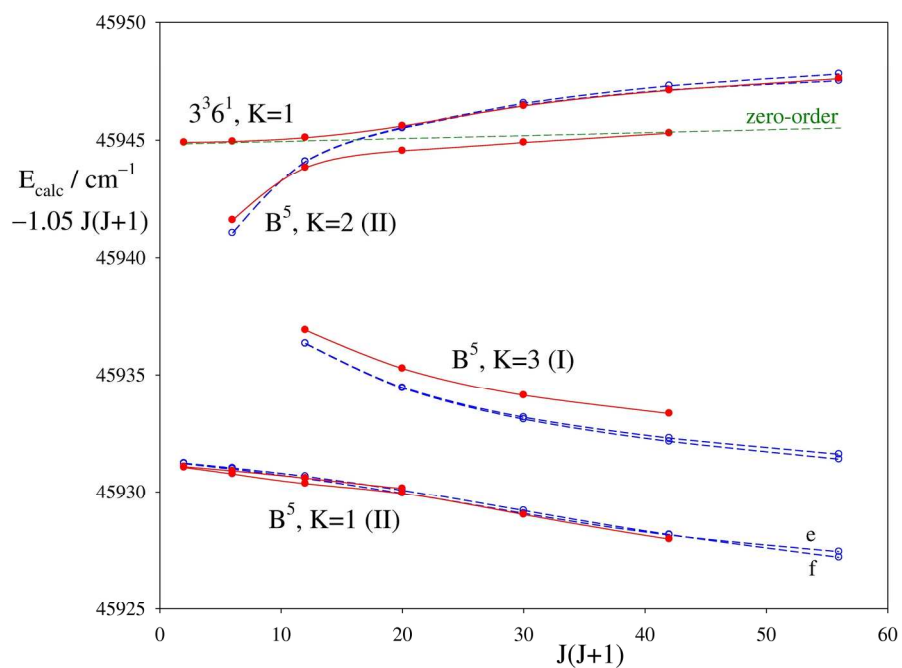


Figure 6 Color  
190x142mm (300 x 300 DPI)

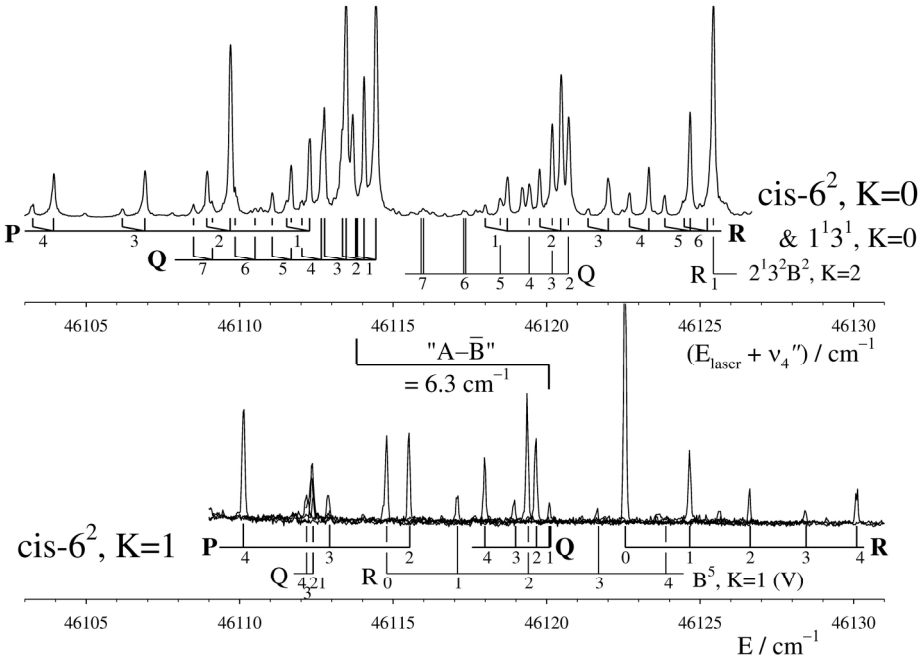


Figure 7 BW  
190x142mm (300 x 300 DPI)

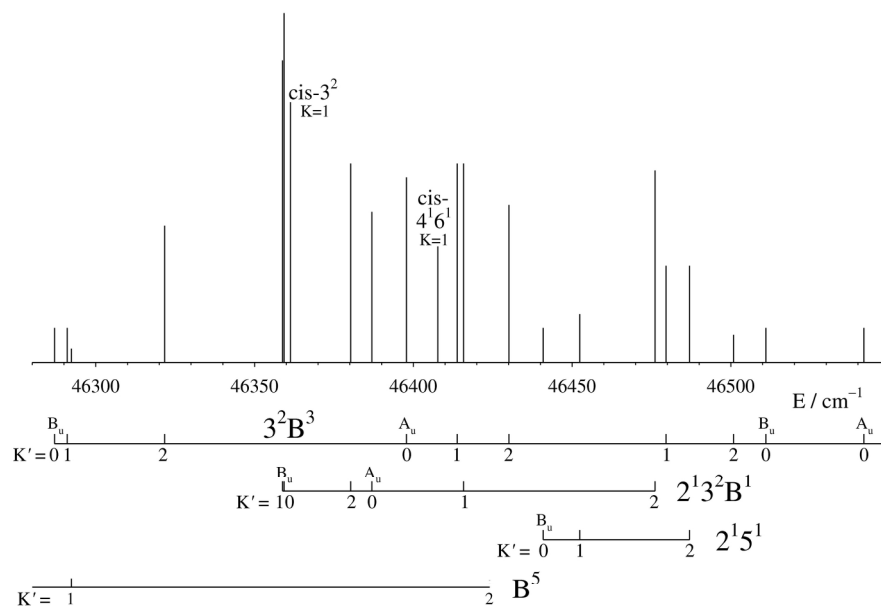


Figure 8 BW  
190x142mm (300 x 300 DPI)



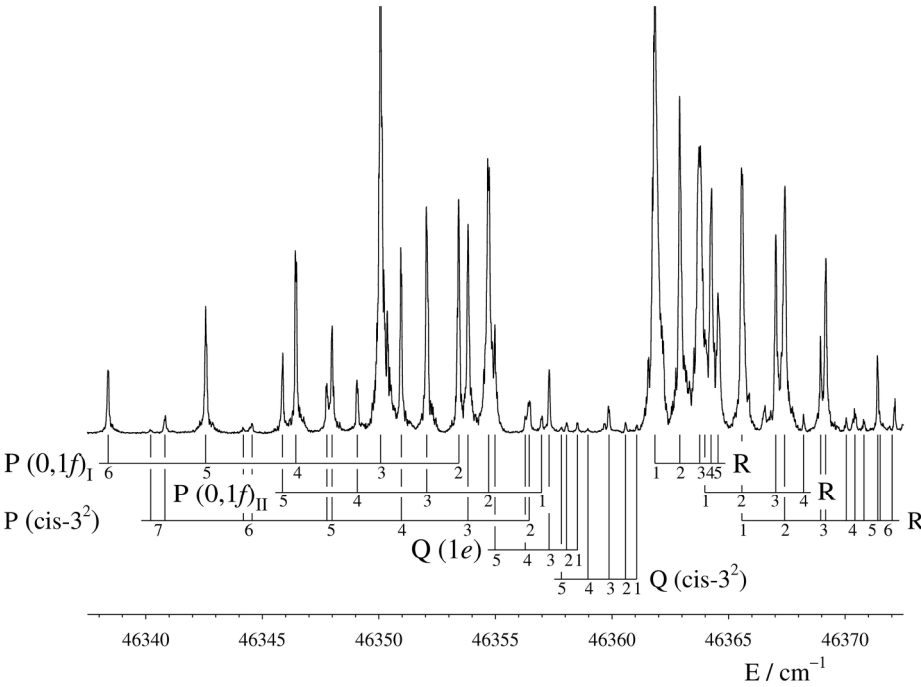


Figure 9 BW  
190x142mm (300 x 300 DPI)

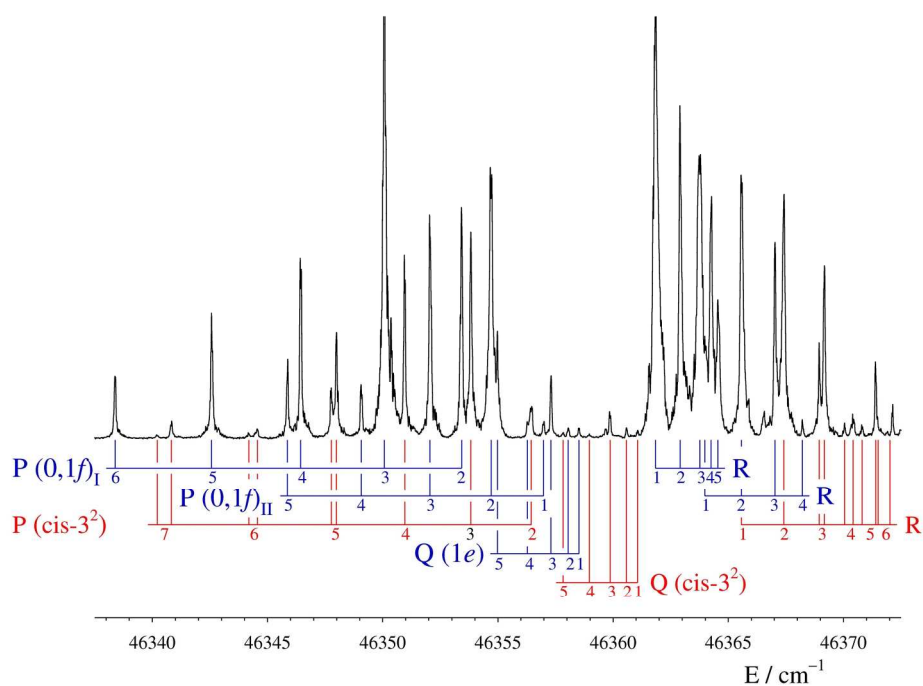


Figure 9 Color  
190x142mm (300 x 300 DPI)

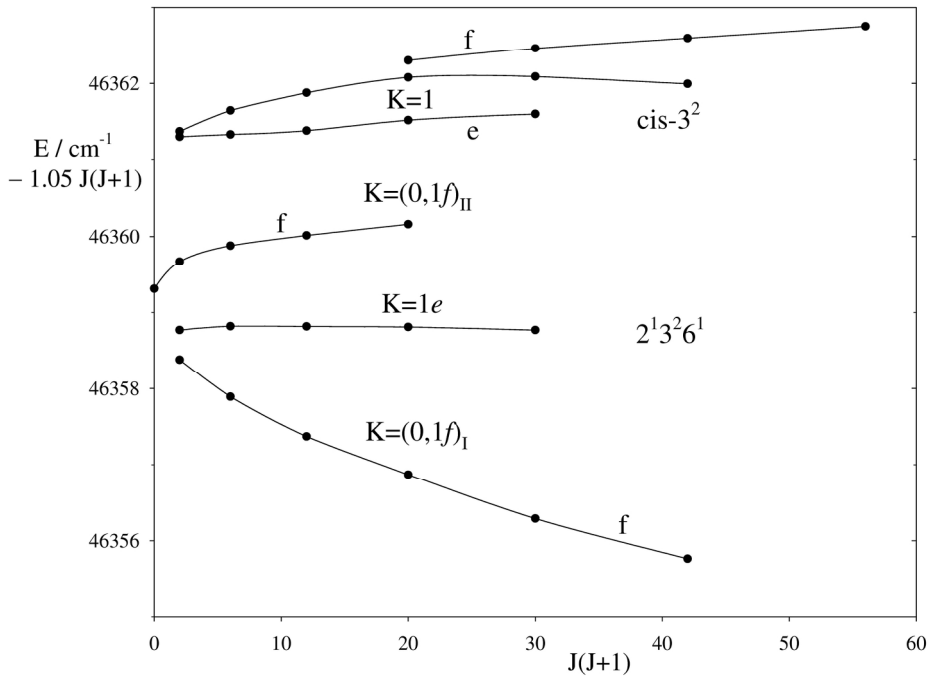
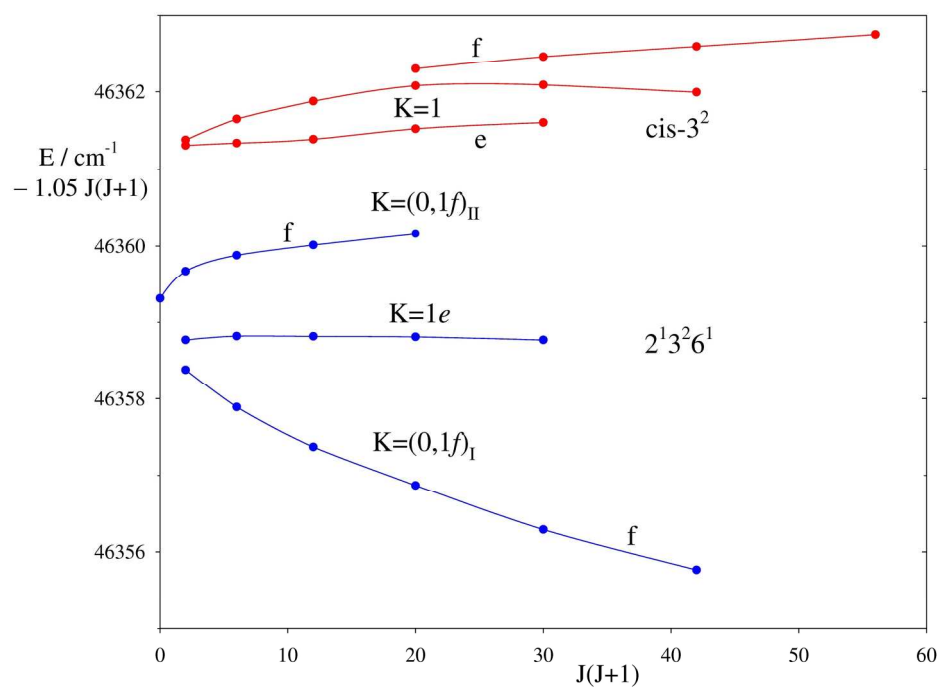


Figure 10 BW  
190x142mm (300 x 300 DPI)



190x142mm (300 x 300 DPI)